Modeling and optimization of a binary geothermal power plant

Citation: Ghasemi, Hadi, Marco Paci, Alessio Tizzanini, and Alexander Mitsos. "Modeling and Optimization of a Binary Geothermal Power Plant." Energy 50 (February 2013): 412–428.

As Published: http://dx.doi.org/10.1016/j.energy.2012.10.039

Publisher: Elsevier

Persistent URL: http://hdl.handle.net/1721.1/104031

Version: Author's final manuscript: final author's manuscript post peer review, without publisher's formatting or copy editing

Modeling and optimization of a binary geothermal power plant

Hadi Ghasemi[a], Marco Paci[b], Alessio Tizzanini[b], Alexander Mitsos[a,*]

[a] *Department of Mechanical Engineering,Massachusetts Institute of Technology,77 Massachusetts Avenue, MIT 3-158,Cambridge, MA,USA*

[b] *ENEL Ingegneria ed Innovazione S.p.A., Area Tecnica Ricerca, Via Andrea Pisano, 120, 56122 Pisa, Italy*

Abstract

A model is developed for an existing organic Rankine cycle (ORC) utilizing a low temperature geothermal source. The model is implemented in Aspen Plus® and used to simulate the performance of the existing ORC equipped with an air-cooled condensation system. The model includes all the actual characteristics of the components. The model is validated by approximately 5000 measured data in a wide range of ambient temperatures. The net power output of the system is maximized. The results suggest different optimal operation strategies based on the ambient temperature. Existing literature claims that no superheat is optimal for maximum performance of the system; this is confirmed only for low ambient temperatures. For moderate ambient temperatures ($T_{amb} \geq 1.7$ ℃) superheat maximizes net power output of the system. The value of the optimal superheat increases with increasing ambient temperature. The optimal operation boosts the total power produced in a year by 9%. In addition, a simpler and semi-analytic model is developed that enables very quick optimization of the operation of the cycle. Based on the pinch condition at the condenser, a simple explicit formula is derived that predicts the outlet pressure of the turbine as a function of mass flow rate of working fluid.

Keywords: Geothermal energy, Organic Rankine cycle, Optimization, Binary plant

*Corresponding Author

Email addresses: hghasemi@mit.edu (Hadi Ghasemi), amitsos@alum.mit.edu (Alexander Mitsos)

Nomenclature

Latin

$\dot{m}^{air}$ Mass flow rate of air in ACC (kg/s)

$\dot{m}^{WF}$ Mass flow rate of working fluid (kg/s)

$\dot{V}$ Volumetric flow rate (m^3/s)

$\dot{W}$ Power (kW)

A_o Total external surface area of root tube (m^2)

A_{tot} Total external surface area of finned tube (m^2)

ACC Air-cooled condenser

C_p^{air} Specific heat capacity of air (J/(kgK))

D Diameter of tube (m)

D_b Bundle diameter (m)

f Friction coefficient

F_b Correction factor for thermosyphon-type circulation

F_p Pressure correction factor

f_f Drive frequency of fan (rpm)

f_p Drive frequency of pump (rpm)

G Mass flux (kg/(m^2s))

GB Geothermal brine

h Specific enthalpy (J/kg)

h_c Heat transfer coefficient (W/(m^2K))

$h_{c,f}$ Heat transfer coefficient of natural convection of liquid (W/(m^2K))

h_{fg} Specific enthalpy of vaporization (J/kg)

L Length of tube (m)

L_B Baffle spacing (m)

N_B Number of baffles

N_s Number of shells

N_T Number of tubes

Nu Nusselt number

P Pressure (Pa)

P_c Critical pressure (Pa)

P_T Tube pitch (m)

Pr Prandtl number

R_D Fouling factor ($(m^2K)/W$)

R_{con} Contact resistance ($(m^2K)/W$)

Re Reynolds number

s Specific entropy (J/(kgK))

T Temperature (℃)

t Thickness of tube (mm)

U_D Overall heat transfer coefficient ($W/(m^2K)$)

W Specific work (kJ/kg)

WF Working fluid

X Specific exergy (J/kg)

x Quality

Greek

ΔT_p Pinch at the vaporizer (℃)

ΔT_{tu} Superheat at inlet of turbine (℃)

η_s Isentropic efficiency of turbine

η_w Weighted efficiency of fin tubes

$\eta_{II,g}$ Geothermal efficiency (Modified second law efficiency of cycle)

η_{II} Second Law efficiency of cycle

η_I Thermal efficiency (First law efficiency of cycle)

κ Thermal conductivity (W/(mK))

μ Viscosity (Pas)

μ_w Viscosity at wall (Pas)

ρ Density (kg/m^3)

Superscript

air air

L Liquid

sat Saturation

V Vapor

Subscripts

max Maximum

min Minimum

amb Ambient

b Boiling

i Inside

n Nozzle

nb Nucleate boiling

o Outer

pa Parasitic

s Shell side

sl Sleeve

tu Turbine

tub Tube

w Wall

1. Introduction

Strategies for the sustainable energy development are based on efficiency improvement in existing energy systems and the introduction of renewable energy sources instead of fossil fuel ones [1]. Although the global contribution of renewable energy systems to the total energy supply is small, due to their potential for sustainability, renewable energy sources have received enormous interest in the last decade. Of particular interest are low and medium temperature thermal energy sources due to their ubiquitous availability. This omnipresence and feasibility of utilization in small-scale power cycles promote decentralized applications of these energy sources. The organic Rankine cycle (ORC) is one of the promising cycles used to extract thermal energy from various energy sources such as solar, biomass and geothermal [2–9].

A thermal energy resource can be characterized by four parameters: reservoir vs stream, temperature (T), rate of energy transfer ($\dot{Q}$) (size) and cost. The characteristics of a thermal energy source affects the optimal choice of working fluid (WF) for an ORC (e.g. [10–20]). Different objective functions have been used for WF selection, such as the ratio of net power output to heat exchanger area ($\dot{W}_{net}$/A) [10], net power output ($\dot{W}_{net}$) [14, 19, 21, 22] and first or second law efficiencies [7, 11–13, 16–18, 20]. Here, we focus on a binary system in which the geothermal stream is in the form of a hot and pressurized liquid, referred to as geothermal brine (GB). The geothermal stream provides thermal energy to the WF of an ORC through a heat exchanger. For these geothermal sources, the first (or thermal) and second-law efficiencies of the ORC can be defined as

$$\eta_I = \frac{\dot{W}_{net}}{\dot{Q}^{GB}} \qquad\qquad \eta_{II} = \frac{\dot{W}_{net}}{\Delta\dot{X}^{GB}}, \tag{1}$$

where $\dot{Q}^{GB}$ denotes the extracted thermal energy by the ORC from the geothermal stream and $\Delta\dot{X}^{GB}$ the exergy difference between the inlet and outlet geothermal streams. In addition to the choice of WF, cycle configuration is another important factor for optimal performance. A common enhancement to the standard Rankine cycle is incorporating an internal heat exchanger

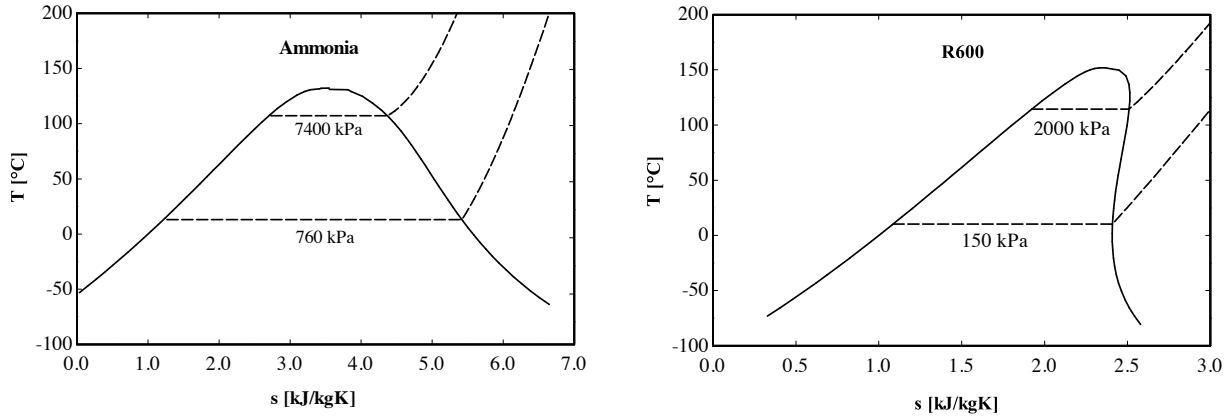

(a) B-type

(b) O-type

Figure 1: A schematic of two types of T-s diagrams are shown. Fluids such as water, ammonia, Pentafluoroethane (R125), Methylene Fluoride (R32), Trifluoroethane (R143a), Chlorodifluoromethane (RE125) are of B-types and fluids such as Octafluoropropane (R218), Pentafluoropropane (R245fa), n-Butane (R600), Isobutane (R600a), n-Pentane (R601) and Isopentane (R601a) fall in the category of O-type.

(recuperator) [23].

WFs are divided in two categories based on the shape of their saturation dome in the T-s diagram: bell-shaped T-s (B-type or normal) which has negative slope of the saturation vapor line for all temperatures (Fig. 1(a)) and overhanging coexistence T-s (O-type or retrograde) which shows a positive slope of the saturation vapor line for a temperature range (Fig. 1(b)) [6]. Typically organic fluids composed of small molecules (Number of C atoms $\lesssim 3$) are mostly of B-type and those consisting of complicated molecules (Number of C atoms $\gtrsim 3$) are mostly of O-Type.

Saleh et al. [6] have suggested different objective functions for choosing a WF for the ORC. They have conducted a pinch analysis for heat transfer between the geothermal brine and WF. Their analysis shows that if the depletion of a geothermal source is taken into account, maximal first law efficiency of the cycle is desired; in contrast, if the outlet GB is discharged to a well, maximum first law efficiency and the minimum outlet GB temperature simultaneously should be taken into account. The minimum outlet brine temperature can be achieved by a second

stage ORC.

Heberle et al. [13] have studied η_I and η_{II} of a binary geothermal ORC with a recuperator with different WFs in the case of $T_{\min}$=15 ℃, $P_{\max} \leq 0.9P_c$ assuming constant isentropic efficiency for both turbine and pump. They have concluded that when η_I is the figure of merit, Isobutane and R245fa are the most suitable WFs for $T_{\max}^{GB}$ ≤167 and $T_{\max}^{GB}$ >167 ℃, respectively; when η_{II} is the figure of merit, two regions are specified. When $T_{\max}^{GB}$ ≤157 ℃, R245fa is the most suitable WF and for higher temperatures of GB, Isobutane is the most suitable one. Saleh et al. [6] have investigated the performance of various WFs in an ORC (with and without a recuperator) with the power output of 1MW using the BACKBONE equation of state. The specifications for the considered case are $T_{\min}$ =30 ℃, $T_{\max}$ ≤100 ℃, $P_{\max} \leq 20$ bar, assuming constant isentropic efficiency of turbine and pump. For subcritical cycles, they have calculated η_I of the ORC with various WFs and have concluded that for all WFs, incorporation of a recuperator improves η_I of the cycle. Moreover, [6] shows that typically O-type fluids offer higher values of η_I than B-type fluids (range of 9.2-14.4 %) because of the low critical temperature and high critical pressure of the organic B-Type WFs. [6] reports that both with or without a recuperator, superheating adversely affects η_I of an ORC with O-type WF. Among the considered WFs, Isobutane, n-Butane, and Isopentane provide maximal η_I with low values of volumetric flow rate through the turbine. Thus, these WFs are suitable candidates for ORCs operating in a subcritical condition and $T_{\max}$ ≤100 ℃. At higher values of $T_{\max}$, n-pentane and n-hexane become better options. Mago et al. [18] have studied the performance of ORC for O-type fluids for the case of $T_{\min}$=25 ℃ and constant isentropic efficiencies of turbine and pump. They have concluded that incorporation of a recuperator increases both η_I and η_{II}. In addition, for both with or without recuperator configurations, higher values of superheat at the inlet of turbine keeps η_I approximately constant and decreases η_{II} due to increase in the irreversibilities.

In conclusion, in the open literature, for subcritical ORC utilizing a low temperature geothermal brine, a cycle with Isobutane and regeneration is considered as a suitable option. These

studies provide a groundwork for further developments of geothermal systems. However, the conclusions on the performance of ORC systems are based on some assumptions and simplifications that may not be satisfied in operating conditions. Thus, a comprehensive analysis on the performance of an ORC is required by taking into account the limitations and performance of the components before making conclusions that can be applied for operating systems with a fixed design. Limitations on isentropic efficiency of turbines (η_s), performance characteristics of pumps and condensation systems can heavily affect the performance of ORCs.

In the current work, a model is developed for an existing commercial ORC with regeneration (using a recuperator) and working with Isobutane as its WF. The condensation system is of air-cooled type. The model includes actual characteristics of all the components including pumps, heat exchangers, turbines, and air-cooled condensers. The heat transfer rates and pressure drop across each component are determined by correlations from the literature and validated using Aspen Exchanger Design & Rating (EDR) models of heat exchangers. The model is implemented in Aspen Plus simulator. The developed model is validated by an available set of data. Optimization of the operation strategies of the ORC is performed by two approaches maximizing $\dot{W}_{net}$: simultaneous multi-variable optimization of the cycle in Aspen Plus and using a new developed approach implemented in EES (Engineering Equation Solver). The new developed model is a fast and shortcut approach for the prediction of optimal operation, but needs some inputs from Aspen Plus simulator. A complete analysis on the performance of the ORC system is performed and new optimal operation strategies are proposed for these systems.

2. Model Development

As aforementioned, the focus of this study is a binary geothermal system utilizing an ORC, shown illustratively in Fig. 2 along with the T-s diagram. Figure 3 shows a more detailed flowsheet of the cycle considered, in particular illustrating the parallel units, e.g., turbines, recuperators and condensers. The process is based on a Geothermal Power Plant operated by ENEL.

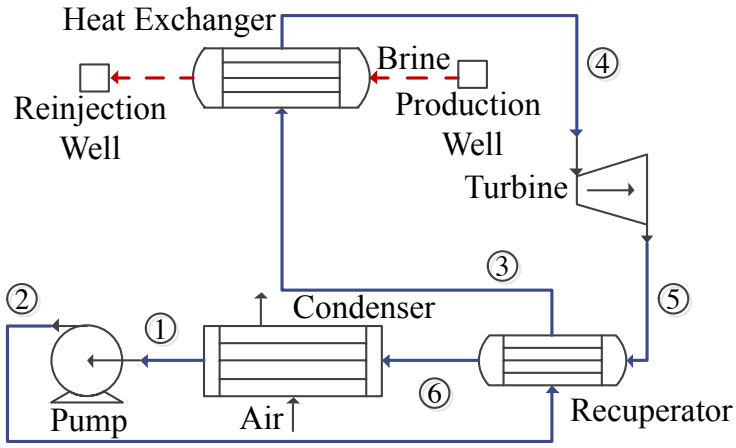

(a)

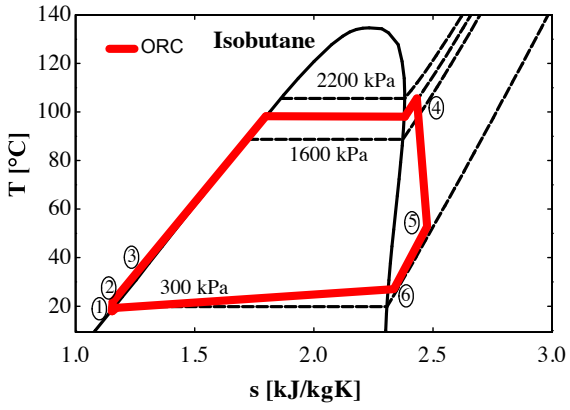

(b)

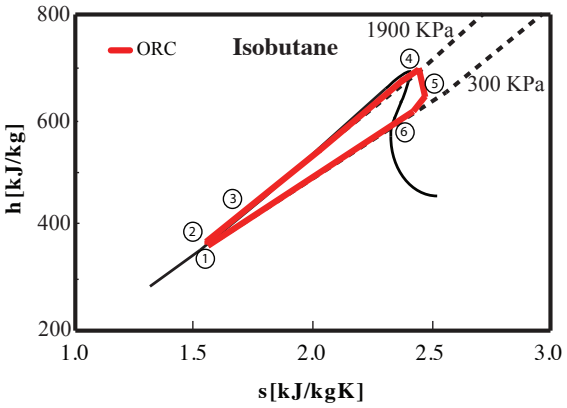

(c)

Figure 2: (a) A schematic of an Isobutane ORC with a recuperator is shown utilizing a low temperature geothermal source. (b) The T-s diagram of Isobutane in the range of temperature and pressure considered in the current study is presented. Since Isobutane is an O-type WF, as shown, the outlet WF of the turbine is always in a superheated state. Note that the inclination of step 6-1 in the diagram is caused by the pressure drop in the condensers. (c) The h-s diagram of Isobutane in the range of extensive properties of the considered system is shown.

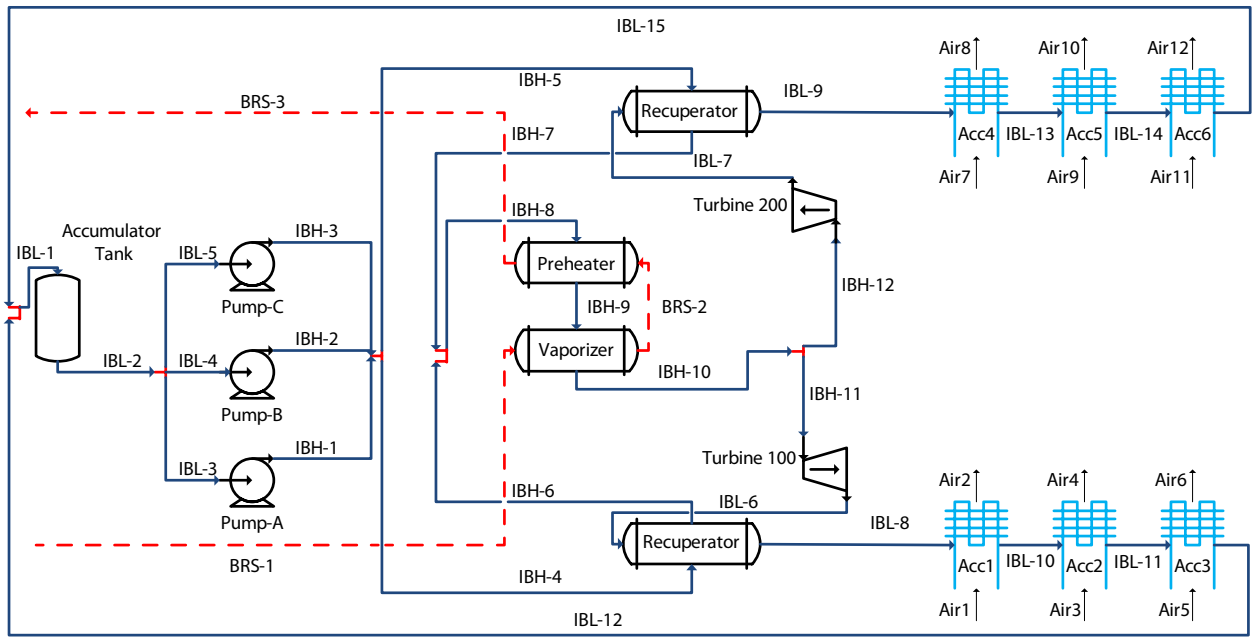

Figure 3: A schematic of the existing ORC in the power plant (ENEL) utilizing a low temperature GB is shown. The inlet temperature and pressure of the GB are T=135 ℃ and P=897 kPa. The WF, the GB and the air streams are depicted in blue (Solid line), red (Dotted line) and black (Arrow), respectively. The system is equipped with three pumps, two of them are constant frequency drive and one is VFD. Two recuperators are used in parallel to preheat the WF. The GB flows through two heat exchangers, vaporizer and preheater, to provide the thermal energy to the ORC. The WF is expanded in turbines each connected to a separate condensation system. The condenser fans are designed as combinations of constant and variable frequency drive systems.

The ORC is modeled using Aspen Plus, a sequential modular flowsheet software. The Equation Oriented (EO) approach in Aspen Plus is another option for the simulation and optimization of a system. This approach in principle is more suitable for optimization, however, in this work, due to the small number of optimization variables, the first approach is considered. The RefProp database is used for the accurate determination of thermodynamic properties in both simulation and optimization of the ORC resulting in relatively large convergence time.

In AspenPlus, the built-in unit operations in the software are used to represent the components of the actual cycle. The schematic of the developed model in AspenPlus is the same as the one shown in Fig. 3. Moving from left to right, the used models are: "Mixer" for the accumulator tank, "Pump" for pumps A, B and C, "HeatX" for the recuperators, preheater and vaporizer, "Compr" for the turbines and "HeatX" for the air-cooled condensers. Design specifications and convergence loops are included in the model as discussed in Section 2.5.

The geothermal source can supply hot brine with the temperature of 135 ℃ and the pressure of 897 kPa. Moving from left to right in Fig. 3, WF stored in an accumulator tank is split into three lines. It is pumped to a high pressure by the three parallel pumps with potentially different flow rates. Two of the pumps use constant frequency drives (Pumps B and C) and one uses variable frequency drive (VFD)(Pump A). For a given drive frequency of a pump, the outlet pressure of the pump depends uniquely on the mass flow rate. The combination of constant frequency drive and VFD systems allows to adjust the mass flow rate and the outlet pressure of the pump independently. For each of the three pumps, correlations between the outlet pressure of the pump and the mass flow rates are obtained and included in the model. The pressurized WFs from the pumps merge together followed by equal splitting to two streams. These two streams flow to two parallel recuperators. The pressurized WFs are on the shell side of the recuperators and superheated vapors exiting each turbine flow through the tube bundles of the recuperators. Thus, the superheated vapors provide thermal energy to the pressurized liquid WFs. The outlet WFs of the two recuperators then mix together and enter to a preheater on the shell side. On the tube side of the preheater, the GB flows. In

the preheating process, a portion of WF may vaporize as well. The preheated WF then enters to the vaporizer on the shell side to go through a phase change process to the vapor phase. The superheat value after the vaporizer is a degree of freedom (DOF). The GB flows through tube sides of the vaporizer and then the preheater to provide the thermal energy to the WF. The outlet GB of the preheater is fed back to the geothermal wells. The superheated vapor phase is split equally into two streams before entering to the turbines. The turbines provide the maximum isentropic efficiency at a specific volumetric flow rate and enthalpy drop of WF across the turbine. The deviation from the maximum isentropic efficiency is discussed below. The thermodynamic path of the current cycle is shown in Fig. 2. Since the WF (Isobutane) is of O-type in the temperature range of this ORC, the outlet WFs of the turbines are in superheated states. The superheated vapors flow through the tube side of recuperators to pass some thermal energy to the liquid WF (regeneration). Then, each vapor stream flows to an air-cooled condensing system (ACC). This type of condensation system is used in arid areas where there is no water source available. However, in general, it offers lower efficiency compared to the water-based condensation systems and its performance is affected significantly by fluctuations of ambient temperature.

The ACC system is composed of two banks of 21 bays with three fans in each bay. Each bank is serving one turbine. In each bay, the last fan is equipped with a constant frequency drive and the two first are VFD. In other words, each bank includes two rows of VFD fans and one row of constant frequency drive fans. The effect of ordering of the fans on the efficiency of the cycle is examined and no measurable effect is found. In each bank, the frequency of VFD fans in each row can be adjusted independent of the other row of VFD fans. As will be discussed in the following, the frequency of the VFD fans and consequently the mass flow rates of air can be adjusted to keep the outlet pressure of the turbines constant. The WF stream flows trough the tubes of ACC system to undergo the phase change process, superheated vapor to sub-cooled liquid. Ambient air is used as the cooling medium and therefore, fluctuations of ambient temperature, T_{amb}, affect the efficiency of the cycle. The condensed WFs from the two

streams merge together and are stored in the accumulator. The ORC is closed and runs in an approximately steady-state condition. The specifications of the ORC and the components are discussed in the following sections.

2.1. Performance of the pumps

As discussed earlier, two of the pumps are equipped with constant frequency drive (1785 rpm) and one of them is VFD. The dependence of pressure rise of a pump on mass flow rate is given by a performance curve. For the pumps in the current ORC, these curves are shown in Fig. 4. As shown, the pressure difference of the pumps are monotonically decreasing functions of the mass flow rates. A constant frequency drive pump has one degree of freedom (ΔP or $\dot{m}^{WF}$). A VFD pump has two degrees of freedom (ΔP and $\dot{m}^{WF}$). However, once the pumps get connected to a system, they loose one degree of freedom since they also have to follow the performance curve of the system. Thus in this pump arrangement herein the only degree of freedom is the frequency of VFD pump. To obtain another degree of freedom, a flow control valve is placed before each pump to control the mass flow rate. We did not account for any pressure drops in the control valves since they are expected to be insignificant. The VFD system uses approximately 5% more electricity than the constant frequency drive systems. The isentropic efficiencies of the pumps as a function of the mass flow rate are shown on the right-hand side axis of Fig. 4. Although the isentropic efficiency of each pump is affected by the mass flow rate and the drive frequency of the pump, considering the low parasitic work of the pumps in this system, this effect can be ignored. The value of $\dot{W}_p$ for the VFD pump has a dependence on both $\dot{m}^{WF}$ and f_p, but for the constant frequency drive pumps, the work is only a function of $\dot{m}^{WF}$.

2.2. Heat transfer coefficients and pressure drops

For each heat exchanger (HX), a HeatX model (Aspen Plus) is used to perform mass and energy conservation analysis. The interval analysis is used for LMTD (Log mean temperature difference) calculations. The area of each HX is given as an input to the model. Two approaches

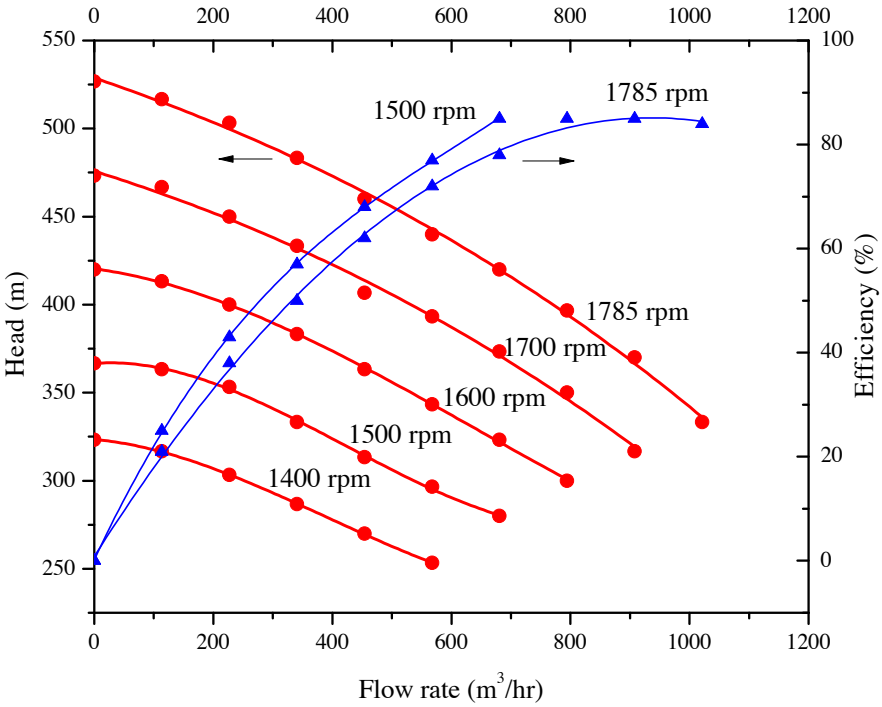

Figure 4: The performance curves of the pumps considered in this study at several drive frequencies are shown. On the left-hand axis, the head of the pump and on the right-hand axis the isentropic efficiencies of the pumps are shown as a function of the mass flow rates. The drive frequencies are given as the labels.

are considered to model the heat exchangers. In the first approach, the available correlations for heat transfer coefficients in the literature are implemented directly into to the simulator. These correlations are given in the Appendix. In the second approach, Aspen Heat exchanger and rating software is used to develop the EDR models. The geometry of the heat exchangers and the fluid properties are the inputs to this software. The specification of the heat exchangers are tabulated in Table 4 in the Appendix. The output of Aspen Heat exchanger and rating software is an EDR file given as an input to the Aspen Plus simulator. This approach is computationally expensive, since in each iteration, the EDR file is read by the simulator and the heat transfer coefficients are recalculated. There is a good agreement between the results of two approaches. Thus, to facilitate the modelling and optimization of the ORC, the first approach is chosen for the rest of study.

2.3. Isentropic efficiency of turbine

For a turbine with given stage pitch diameter and turbine rotational speed, the isentropic efficiency is a function of volumetric flow rate of WF and enthalpy drop through the turbine [24]. The isentropic efficiency of the turbines is obtained from manufacturer data. For these turbines, the maximum value of η_s is 86 %. However, as discussed in the following, deviations of operating condition from this maximum adversely affects the performance of the turbine and consequently η_s. This deviation can be expressed as a function of ratio of enthalpy drop (r_T) and ratio of volumetric flow rate (r_{VT}) [24]. For the considered turbine in this study, the dependence of η_s on these parameters is written as

$$\begin{aligned} r_T &= \sqrt{(h_4 - h_5)/(h_4 - h_5)^{max}} \\ r_h &= ([(1.398 r_T - 5.425) \times r_T + 6.274] \times r_T - 1.866) \times r_T + 0.619, \end{aligned} \tag{2}$$

where h_I, (I=1..6) denote the enthalpies of the state shown in Fig. 2 and

$$\begin{aligned} r_{VT} &= (\dot{V})/(\dot{V})^{max} \\ r_v &= ([(-0.21 r_{VT} + 1.117) \times r_{VT} - 2.533] \times r_{VT} + 2.588) \times r_{VT} + 0.038. \end{aligned} \tag{3}$$

Then, the isentropic efficiency of the turbine can be expressed as

$$\eta_s = 0.86 \times r_h \times r_v \tag{4}$$

Also by its definition, η_s can be expressed as

$$\eta_s = \frac{h_4 - h_5}{h_4 - h_5^s} \tag{5}$$

If for a turbine, inlet and outlet states are fixed during an operation, assumption of constant η_s holds. However, for most of the operating turbines in ORCs, condensation systems are of air-cooled type and thus the condenser pressure is significantly affected by air temperature and consequently the performance of the turbine varies a lot. Hence, assumption of constant η_s does not resemble real performance of turbine. For instance, the isentropic efficiency of the turbine considered in this study with a fixed inlet condition is plotted as a function of outlet pressure in Fig. 5. Dependence of the power of turbine on the outlet pressure is also included in Fig. 5. As shown, there is an optimum pressure for the maximum power output of turbine. Deviation from this pressure affects the power of turbine adversely. This effect is more remarkable at low outlet pressures of turbine. In contrast, if the isentropic efficiency is constant, a monotonic increase in power output as the outlet pressure decreases is obtained. Thus, a constant isentropic efficiency is not only quantitatively wrong, but gives qualitatively different results; to simulate the actual performance of a turbine, the correlation of isentropic efficiency should be implemented in the model.

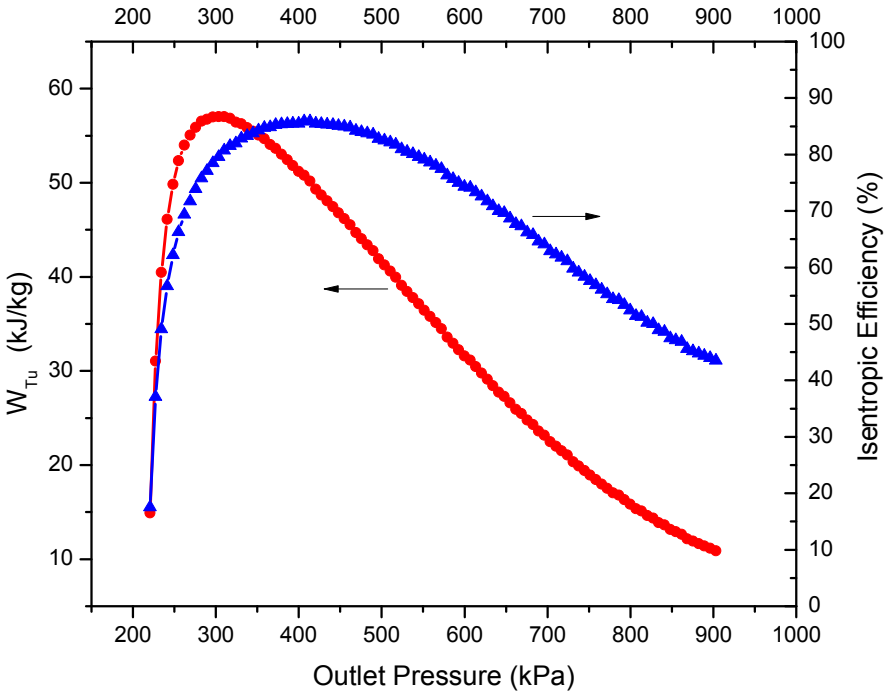

Figure 5: The isentropic efficiency curve of the turbine considered in this study is shown as a function of the outlet pressure on the right-hand side axis. This turbine is designed for an ORC with Isobutane as its WF. This curve is calculated for a fixed inlet state: $\dot{m}^{WF}$= 201.60 kg/s, T_4=101.11 ℃ and P_4=1654.74 kPa. Also, the corresponding power of turbine is shown on left-hand side axis. Note that the maximum in isentropic efficiency and power output are obtained at different outlet pressures.

2.4. Air-cooled condensers (ACC)

As pointed out earlier, the ACC system consists of two parallel banks. A discussion on the number of fans in each bank will be presented later. The exhaust WF from each recuperator, is split between bays and passes through three fans in series. At the outlet of the ACC system, the WF must be in a liquid state. A value of 0.625 ℃ sub-cooling is specified to satisfy this requirement. The heat transfer coefficients and the pressure drop across the ACC is determined by the procedure discussed above (Section 2.2). The ACC system is modelled with two sets of three condensers that each represent a row of 21 fans. In the current model, the surface areas of the ACCs are fixed.

2.5. Implementation of the design and operation

For the given design in Fig. 3, the characteristics of the components of the system are obtained and implemented in the model. These characteristics along with the operation strategies determine $\dot{m}^{WF}$, T_5 and P_5 (see Fig. 2(a)) Two operation strategies will be considered: the base case (i.e., the current operation) and the optimal operation.

The $\dot{m}^{WF}$ in the ORC is such that the value of superheat after the vaporizer is equal to the pre-specified value, 8 ℃ in the base case. The value of T_5 is determined once the correlation for η_s is included in the model. This correlation suggests that for a given (T_4,P_2), once P_5 is obtained, η_s is fixed and it determines the value of T_5 by an iterative procedure. The iteration scheme used is Bisection method. After guessing T_5, the right hand sides of Eq. 2 to 4 are evaluated. The iteration is repeated until η_s calculated in Eq. 4 matches that in Eq. 5. Two sets of specifications are introduced to determine P_5. The cooling capacity of the ACC system is a function of T_{amb} and frequency of the fans (f_f). First it is defined that for a given cooling capacity of ACC, P_5 is such that the WF after the ACC has 0.625 ℃ subcooling. The cooling capacity of the air-cooled condensing system is limited and it cannot provide any desired value of P_5. As remarked above, Fig. 5, the power output of the turbine has an optimum at a specific value of P_5. Thus, if possible, one should operate the system at this optimum point. However, this type of operation can only be achieved if T_{amb} and f_f provide the possibility

to have sufficient cooling capacity without disporportionate parasitic load. To introduce the second set of specifications in the model, we have divided the operation of the system to two regions based on the determined value of P_5 from the first specification. For a given T_{amb}, if $P_5 \leq P_{opt}$ at the maximum load of the fans (maximum f_f), the cooling capacity is lowered to keep $P_5 = P_{opt}$. Otherwise the ACC system works at the maximum load. The adjustment to the cooling capacity of the ACC system is achieved by the incorporation of VFD fans in this model. The flow rate of air through the fans can be determined once the performance curves of the fans are available. These performance correlations are included in the model via design specifications in AspenPlus. By using these correlations, for a specific f_f, and given air densities in the inlet and outlet of the ACC, the mass flow rate of the air can be determined.

Once these design characteristics and operation strategies are introduced, two sets of calculator blocks are introduced in Aspen Plus. The first set determines intermediate variables needed to be supplied to the simulator. These include the air flow rates through fans, the heat transfer coefficients and the pressure drops. The total flow rate of air can be obtained from the given correlations of fans. The introduced correlations for the heat transfer coefficients and the pressure drop are introduced as calculator blocks for each component. The second set of calculator blocks is used to post-process the results, i.e., to determine the mass flow rate through each pump, parasitic work ($\dot{W}_{pa}$) and efficiencies of the ORC.

Since the sequential modular approach is used to simulate the system, the loops in the ORC (Fig. 3) are replaced by tear streams. At the two side of the tear streams, two independent thermodynamic variables (here, pressure and temperature) must be equal. This condition for each tear stream is included in the design specifications. Three convergence blocks are defined: in the first block, all the design specifications pertaining to the ACC system and the outlet pressure of turbine (P_5) are included to be converged together; in the second one, it is specified that the two parallel inlet streams (Liquid streams) to the recuperators are converged together; and in the last block, it is specified that two tear streams exiting the recuperators (Liquid streams) are converged together.

3. Model validation and analysis of the operation

The values of T_{amb}, T_{BRS-1}, T_{BRS-3}, $\dot{m}_{br}$ and P_2 are the input parameters to the model. Once these values are specified, the model determines the thermodynamic states of WF through the cycle, the net power output ($\dot{W}_{net}$) and the efficiencies based on the operation strategy selected. Note that the parasitic power of brine production and reinjection pumps are also included. A set of approximately 5000 data points from the power plant (ENEL) is obtained that includes the net power output and the thermodynamic state of WF at various points in the cycle. This set of data is used to validate the developed model and the comparison is shown in Fig. 6 as a function of T_{amb}. In this figure, one can distinguish two regions for the power output of turbine. When T_{amb} is less than 1.7 ℃, the net power output of the plant is approximately constant. In this region, as discussed above, f_f of VFD fans are adjusted to keep P_5 constant. If T_{amb} is more than 1.7 ℃, all the fans are working at the full load and the cooling capacity of the system governs P_5 and consequently $\dot{W}_{net}$. In this set of measured data, there are some off-operation points, i.e., points that do not follow the operating strategy. These points offer lower values of the net power output compared to the base-case operations. These points are caused by the interruptions in the performance of the ORC, e.g. replacement of turbine gaskets.

The developed model is examined further by evaluation of thermodynamic properties of the WF at intermediate states. The measured outlet temperature of GB is compared with the values predicted by the model and shown in Fig. 7.

In a geothermal binary plant, the brine provides thermal energy to the ORC and it is discharged to wells afterwards. The geothermal brine is an aqueous solution of various minerals. Depending on the temperature and pressure of the brine, these components can precipitate and/or form other phases. The new phases are in the form of solid precipitate in the heat exchangers (causing fouling) which adversely affect the heat transfer rates. Thus, the temperature and pressure of brine should be kept in a range that liquid solution is the only thermodynamic stable phase. For the considered system, the outlet temperature of GB should be no less than 60 ℃ before discharging to the wells.

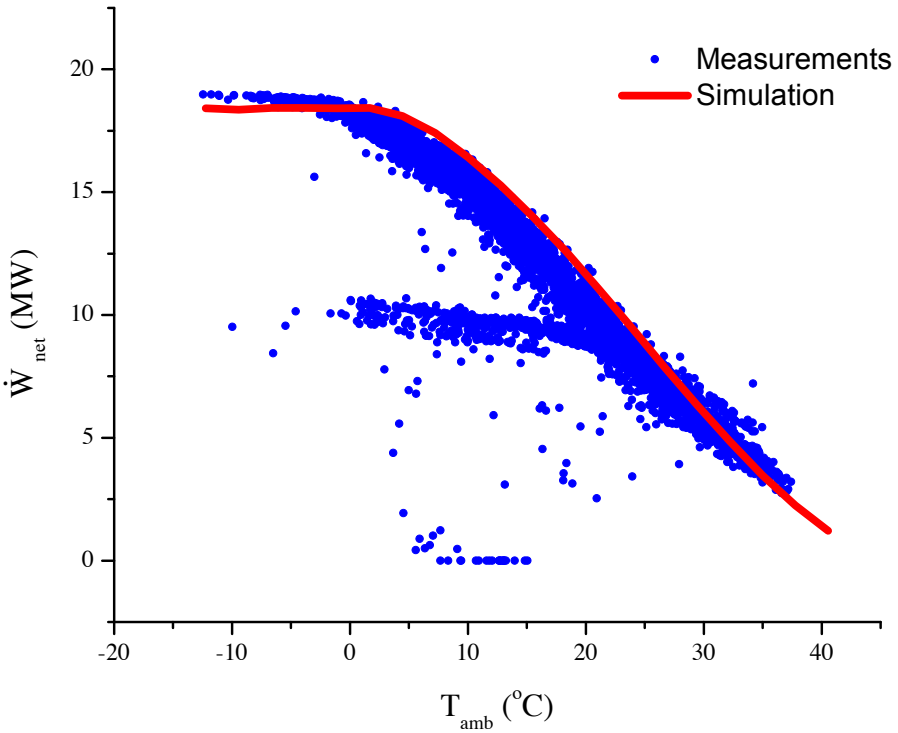

Figure 6: The simulated values of $\dot{W}_{net}$ (line) are compared with the measured ones (dots). The measurements are divided in to two categories: the measurements in the base-case operation with a good agreement with the simulated values and the off-operation measurements. These off-operation data are measured during the maintenance of one of the turbines and thus give lower values of $\dot{W}_{net}$ at a given T_{amb}.

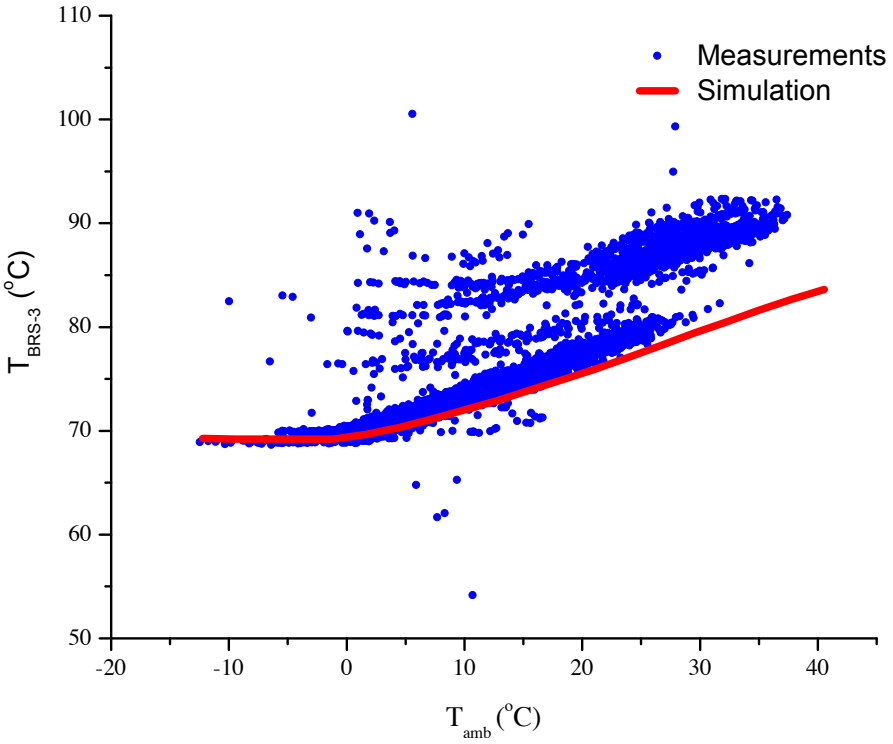

Figure 7: The simulated values of outlet temperature of GB (line) is compared with the measured ones (dots). For a fixed operation, the value of thermodynamic properties should be constant for a given T_{amb}. However, due to off-operation and error in the measurements, different values of T_{BRS-3} are measured for a given T_{amb}. On the base-case operation, the simulated results represent the measured data with a good accuracy.

The performance of the cycle is evaluated based on thermal and geothermal efficiencies (first and modified second law efficiencies). The thermal efficiency (Eq. 1) may be rewritten as

$$\eta_I = \frac{\dot{W}_{net}}{\dot{m}^{GB} \times (h_{in}^{GB} - h_{out}^{GB})}, \tag{6}$$

and geothermal efficiency (modified Eq. 1) may be defined as

$$\eta_{II,g} = \frac{\dot{W}_{net}}{\dot{m}^{GB} \times (X_{in}^{GB} - X_{\min}^{GB})}, \tag{7}$$

where X_{in}^{GB} and $X_{\min}^{GB}$ denote the inlet exergy and minimum outlet exergy before reinjection to the wells, respectively. The values of η_I, $\eta_{II,g}$ and η_s of turbine for a range of T_{amb} are shown in Fig. 8 for base-case operation. The η_I of the ORC varies in the range of 1-11 %. When $T_{amb} \leq 1.7$ ℃, the inlet and outlet state of the turbine is fixed (P_5 is kept at the optimal value for maximal η_s of turbine); thus η_I is approximately constant. Note that although the parasitic work of fans increases monotonically as a function of T_{amb} in this range, its contribution is negligible in $\dot{W}_{net}$. At $T_{amb} \geq 1.7$ ℃, although the inlet state of the turbine is fixed, the outlet state is affected by the cooling system and η_I is a monotonically decreasing function of T_{amb}. With respect to $\eta_{II,g}$, there is an optimum at T_{amb}= 1.7 ℃. The available exergy to the system ($X_{in}^{GB} - X_{\min}^{GB}$) is a monotonically decreasing function of T_{amb} based on exergy formulation. When $T_{amb} \leq 1.7$ ℃, the value of $\dot{W}_{net}$ is constant, and thus $\eta_{II,g}$ decreases. For $T_{amb} \geq$1.7 ℃, $\eta_{II,g}$ is a decreasing function of T_{amb}, since $\dot{W}_{net}$ is the dominant parameter in $\eta_{II,g}$. Concerning η_s, there is a maximum at $T_{amb} \approx 10$ ℃. This maximum corresponds to the maximum of η_s in Fig. 5.

In conclusion, the comparison of model prediction with the measured data from the existing plant validate the developed model. Note that no parameter fitting was performed. The developed model is used in the next section for the optimization by altering the operation strategy.

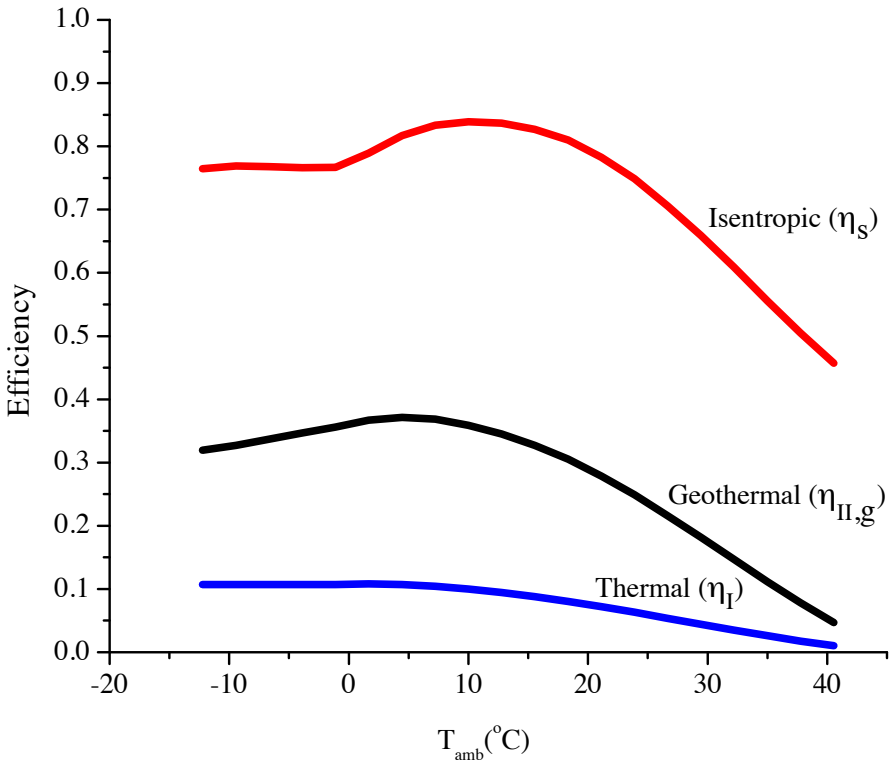

Figure 8: For the considered ORC in Fig. 3, the values of η_I, $\eta_{II,g}$ and η_s of turbine for a range of T_{amb} at the base-case operation are shown. The η_I and consequently $\dot{W}_{net}$ of the system offer maximum values at low ambient temperatures.

4. Effect of number of fans on optimal performance

There are some possibilities to boost the performance of the system. One of the constraints on the output power of the system is caused by the design of the ACC system. It is found that P_5 is a function of cooling capacity of the ACC system. If T_{amb} is more than 1.7 ℃, P_5 is fixed for a given T_{amb} and it limits the value of the net power output of the ORC. One approach for releasing this constraint is to increase the cooling capacity of the ACC system by incorporating more fans in the system. This idea is explored (to disclose the effect of ACC system on the cycle performance and as a benchmark for optimization of operation) by introducing one or two more fans in each bay. Although by taking this approach the parasitic load ($\dot{W}_{pa}$) in the system will be increased, this increase is very small compared to the increased turbine power output. For comparison, also the case of reducing the number of fans to two is considered. The findings are shown in Fig. 9. When T_{amb} is less than 1.7 ℃, the extra fan in each bay has no contribution and should be turned off. However, when T_{amb} is more than 1.7 ℃, introducing more fans and raising the cooling capacity of the system shows a major contribution to the power output of the ORC. For instance, at T_{amb}=32.2 ℃, systems with 4 and 5 fans in each bay offers 49% and 77% increase in the $\dot{W}_{net}$, respectively. The optimal number of fans depends on the capital cost and can only be determined by a thermoeconomic analysis. The goal herein is to achieve similar increase in performance for high ambient temperatures for a fixed design by optimizing the operation.

5. Optimization of the operation of the ORC

Once the model is validated, the model is examined to obtain the optimum operating parameters and strategy for the system. As discussed above, if depletion of a geothermal source is ignored, one can consider the source as a continuous stream of thermal energy. Thus, as long as the minimum outlet temperature and pressure of brine are satisfied, the maximum power output of the system (more important) with minimal flow rate of brine is favorable. In the current study, the mass flow rate of brine is assumed constant. Thus, the maximum power

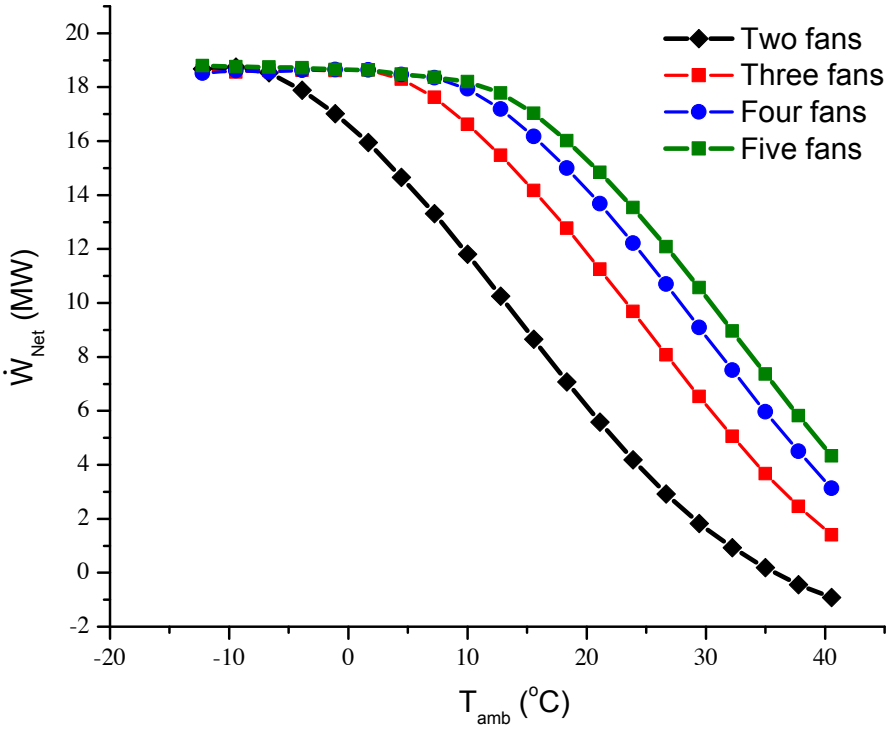

Figure 9: The performance of the ORC in different configurations of the ACC system are compared: two, three, four and five fans in each bay. The results suggest that increase in the cooling capacity of the system can significantly affect the performance of the system at high T_{amb}.

output of the system is chosen as the objective function. The net power of the ORC is the power produced by the turbines subtracted by the parasitic work of the system. The parasitic work of the system which includes the work of the pumps and the fans of ACC may be written as

$$\dot{W}_{pa} = \dot{W}_p^{WF}(\dot{m}^{WF}) + \dot{W}_f(\dot{V}_{air}, f_f) + \dot{W}_p^{GB}(\dot{m}^{GB}) \tag{8}$$

and,

$$\dot{W}_{net} = \dot{W}_{tu}(\dot{m}^{WF}, T_4, P_4, T_5, P_5) - \dot{W}_{pa}(\dot{m}^{WF}, \dot{V}_{air}, f_f, \dot{m}^{GB}) \tag{9}$$

Six constraints are applied by the current design of the ORC. First, P_5 is limited by the design of the ACC system, $P_5 = P_5(T_{amb}, f_f)$. Secondly, the isentropic efficiency of the turbine correlates the inlet and outlet states of the turbine, $g(\dot{m}^{WF}, T_4, P_4, T_5, P_5) = 0$. Thirdly, the pinch at the vaporizer correlates the mass flow rate of WF and superheat after the vaporizer, $\dot{m}^{WF} = \dot{m}^{WF}(T_4, P_2)$. Fourthly, the volumetric flow rate of air through the ACC system depends on the ambient temperature and the drive frequency of the fans, $\dot{V}_{air} = \dot{V}_{air}(T_{amb}, f_f)$. Fifthly, the value of P_4 is determined by P_2 and pressure drop through the components which is a function of $\dot{m}^{WF}$. Finally, the WF at the inlet of turbine should be in a superheated state. The optimization problem can be formulated as

$$\begin{aligned}
\max_{\dot{m}^{WF}, T_4, P_2, T_5, P_5} \quad & \dot{\mathrm{W}}_{\mathrm{net}}(T_{amb}, \dot{m}^{WF}, T_4, P_2, T_5, P_5, \dot{V}_{air}, f_f, \dot{m}^{GB}) \\
\text{s. t.} \quad & P_5 = P_5(T_{amb}, f_f) \\
& g(\dot{m}^{WF}, T_4, P_4, T_5, P_5) = 0 \\
& \dot{m}^{WF} = \dot{m}^{WF}(T_4, P_2) \\
& \dot{V}_{air} = \dot{V}_{air}(T_{amb}, f_f) \\
& P_4 = P_4(\dot{m}^{WF}, P_2) \\
& T_4 \geq T^{sat}(P_4)
\end{aligned} \tag{10}$$

This problem is a parametric optimization in terms of T_{amb}. For this optimization problem,

one can reformulate the problem and redefine the feasible set by implementing some of the constraints as design specifications in the model, i.e., solving for them at the simulation level. The approach for redefining the feasible set is successfully used in [25] as well. For the problem at hand the taken approach helps to solve the problem without need for optimization. The first constraint represents the effect of the cooling capacity on P_5. As discussed in the modelling section, this constraint can be implemented as two sets of design specifications. The second constraint represents the performance of the turbine. For a given volumetric flow rate, the η_s correlation of the turbine relates the thermodynamic state of the inlet and outlet of the turbine. In the design specification section, it is defined that for a given state 4 (T_4,P_4) of the WF and P_5, the value of T_5 should be such that to satisfy the equation of η_s of the turbine. This equation is implemented as a FORTRAN code into the model. The third constraint specifies $\dot{m}^{WF}$. In the current configuration of the ORC with the given surface area of heat exchangers, the value of $\dot{m}^{WF}$ depends on the thermodynamic state of WF at state 4. For a given P_2 and a pre-defined value of superheat, $\dot{m}^{WF}$ should be adjusted to satisfy the conservation of energy in the heat exchangers. Although f_f is a DOF in this problem, for the current design, it is only a variable at low ambient temperatures. When $T_{amb} \geq 1.7$ ℃, the optimal value of f_f is the maximal, 242 rpm. However, when $T_{amb} \leq 1.7$ ℃, f_f can be considered as a DOF. The optimal value of f_f at the low ambient temperatures will be discussed later. Consequently, for a given T_{amb}, $\dot{V}_{air}$ is considered fixed. Also, the value of $\dot{m}^{GB}$ is fixed in this system. Instead of T_4, the value of superheat at state 4 is defined as a new variable, $\Delta T_{tu} \geq 0$. This modification to the independent variables guarantees that the last constraint is satisfied. Hence, by transferring the constraints to the design specification section, one can reformulate the optimization problem. By implementing these design specifications, the optimization problem can be written as a box-constrained optimization problem

$$\begin{aligned} \max_{\Delta T_{tu}, P_2} \quad & \dot{\mathrm{W}}_{\mathrm{net}}(T_{amb}, \Delta T_{tu}, P_2) \\ \text{s. t.} \quad & \Delta T_{tu} \geq 0 \\ & 1792 \leq P_2 \leq 2137 \quad kPa \end{aligned} \tag{11}$$

The range of P_2 is based on the performance curve of the pumps. For a given drive frequency of pump, maximal P_2 corresponds to the minimum in the flow rate of WF through each pump (to have a continuous stable flow) and minimal P_2 is given by the maximum flow rate of WF through the pump. For the specified range of P_2, the mass flow rate of WF is implied to be in the range of 273-1000 kg/s.

Two approaches are used to solve this optimization problem. In the first approach, the feasible set is discretized, i.e., the optimization problem is solved with the brute force method. This approach guarantees the approximate global solution of the problem and shows that the objective function is unimodal. In the second approach, the SQP optimizer built-in in Aspen Plus is used which solves for a local solution of the problem. Since the objective function is unimodal, the SQP local solver gives the same solution as the discretization approach.

5.1. Optimization results

At the ambient temperature of -1.11 ℃, the optimization problem is solved with the first approach and the results are shown in Fig. 10. This figure suggests that the maximum value of $\dot{W}_{net}$ is reached if the turbine inlet (state 4, Fig.2), corresponds to the saturated vapor at the maximum feasible pressure. This result is in agreement with [6], but also demonstrates that the current operation is not optimal.

The net power produced at the optimum point is 3.8% more than the current operating condition. Furthermore, the value of efficiencies as a function of independent variables are shown in Fig. 11. The results suggest that η_s is almost independent of superheat condition and an increasing function of pressure. As discussed, at a given T_{amb}, $\eta_{II,g}$ only depends on $\dot{W}_{net}$ and is maximum when the power output is maximum. In contrast, η_I shows a maximum at

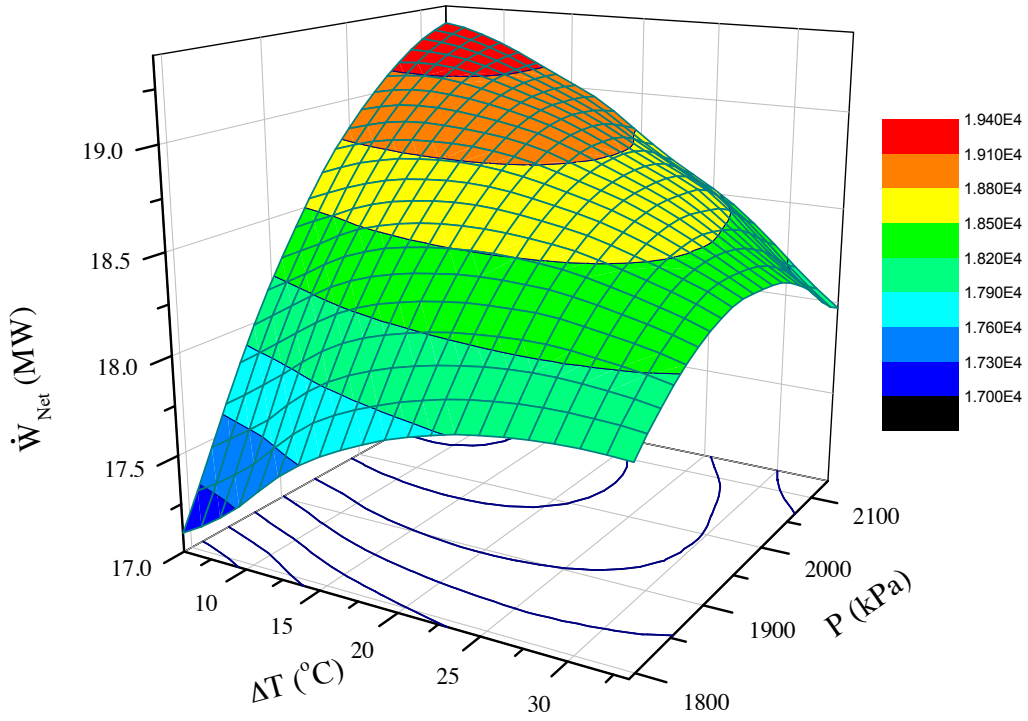

Figure 10: The value of the net work as a function of the two independent variables, ΔT_{tu} and P_2 is shown for ambient temperature of -1.11 ℃. The contour of the objective function is plotted on the X-Y plane.

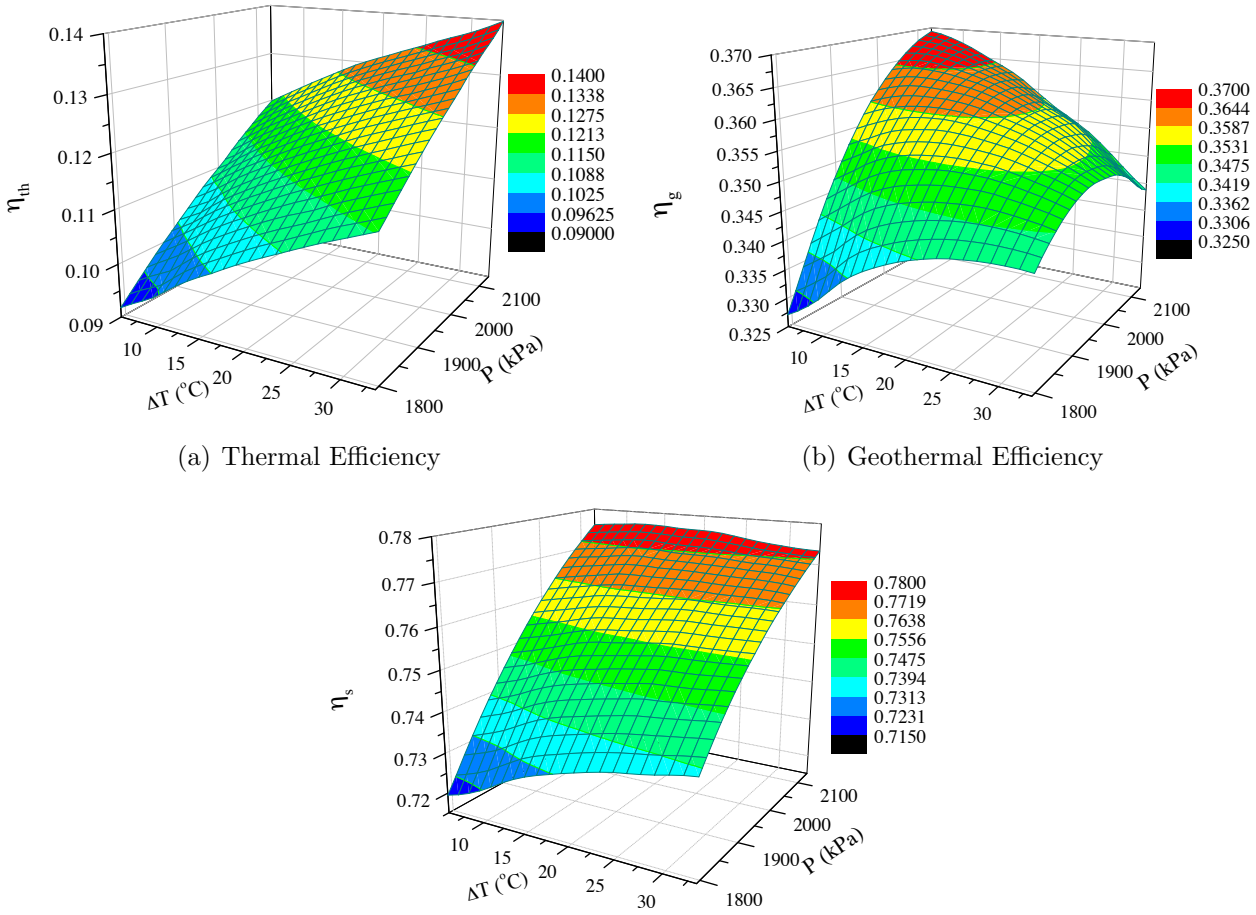

(a) Thermal Efficiency

(b) Geothermal Efficiency

(c) Isentropic Efficiency

Figure 11: The values of η_I, $\eta_{II,g}$, and η_s of turbine are shown as functions of the two independent variables at T_{amb}=-1.11 ℃. The colored mesh represents the magnitude of the efficiencies.

the maximum feasible ΔT_{tu} and P_2, i.e., its maximum does not coincide with the maximum of $\dot{W}_{net}$.

The optimization problem is also solved for the ambient temperature of 26.7 ℃ and the results are shown in Fig. 12. For this high ambient temperature, the maximum of the net work is attained when state 4 is placed at the maximum feasible pressure and close to maximum superheat. This finding is in contrast to the previous works in the literature [6, 18] which claimed that maximal net work of ORC is obtained for no superheat at the turbine inlet. The value of objective function in this case can be increased by 30.6% if the operating conditions

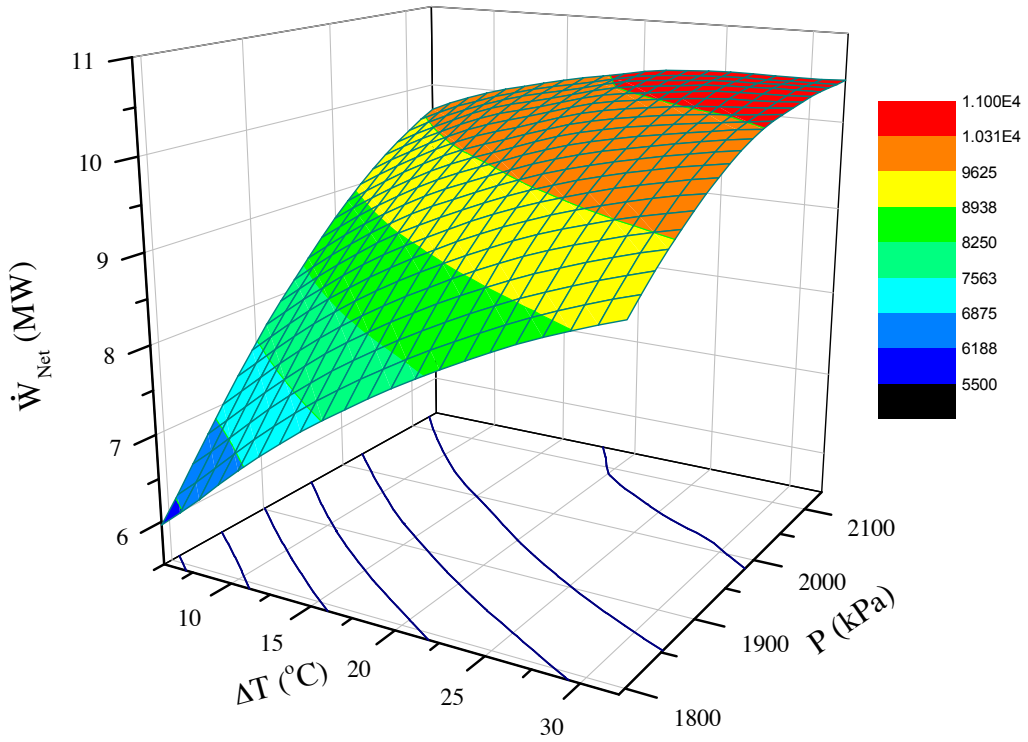

Figure 12: The value of the net work is plotted as a function of the two independent variables for T_{amb}=26.7 ℃. The maximum is attained close to the boundary of the feasible set. Note that the maximum occurs close to the different corner of the feasible set compared to Fig. 10.

are moved to the optimum point. Furthermore, the values of η_I, $\eta_{II,g}$, and η_s of the turbine for the case of T_{amb}=26.7 ℃ is shown in Fig. 13.

The comparison of the optimal conditions for the two temperatures is of importance. Although the maximum of the objective function occurs at the maximum value of feasible pressure in both cases, the values of optimal superheat differ in these cases. These results suggest different optimum operation strategy based on T_{amb}. The presented results suggest that depending on T_{amb}, the ORC should be operated by different rules. This finding is investigated further by determining the objective function at the maximum feasible P_2 for a range of ΔT_{tu} as a function of T_{amb}. The results are shown in Fig. 14(a). The values of ΔT_{tu} are included for some optimum conditions. Note that for $T_{amb} \leq 10$ ℃, the optimal ΔT_{tu} is zero; for $T_{amb} > 10$ ℃, optimal ΔT_{tu} increases continuously with T_{amb} and finally reaches to a plateau given by

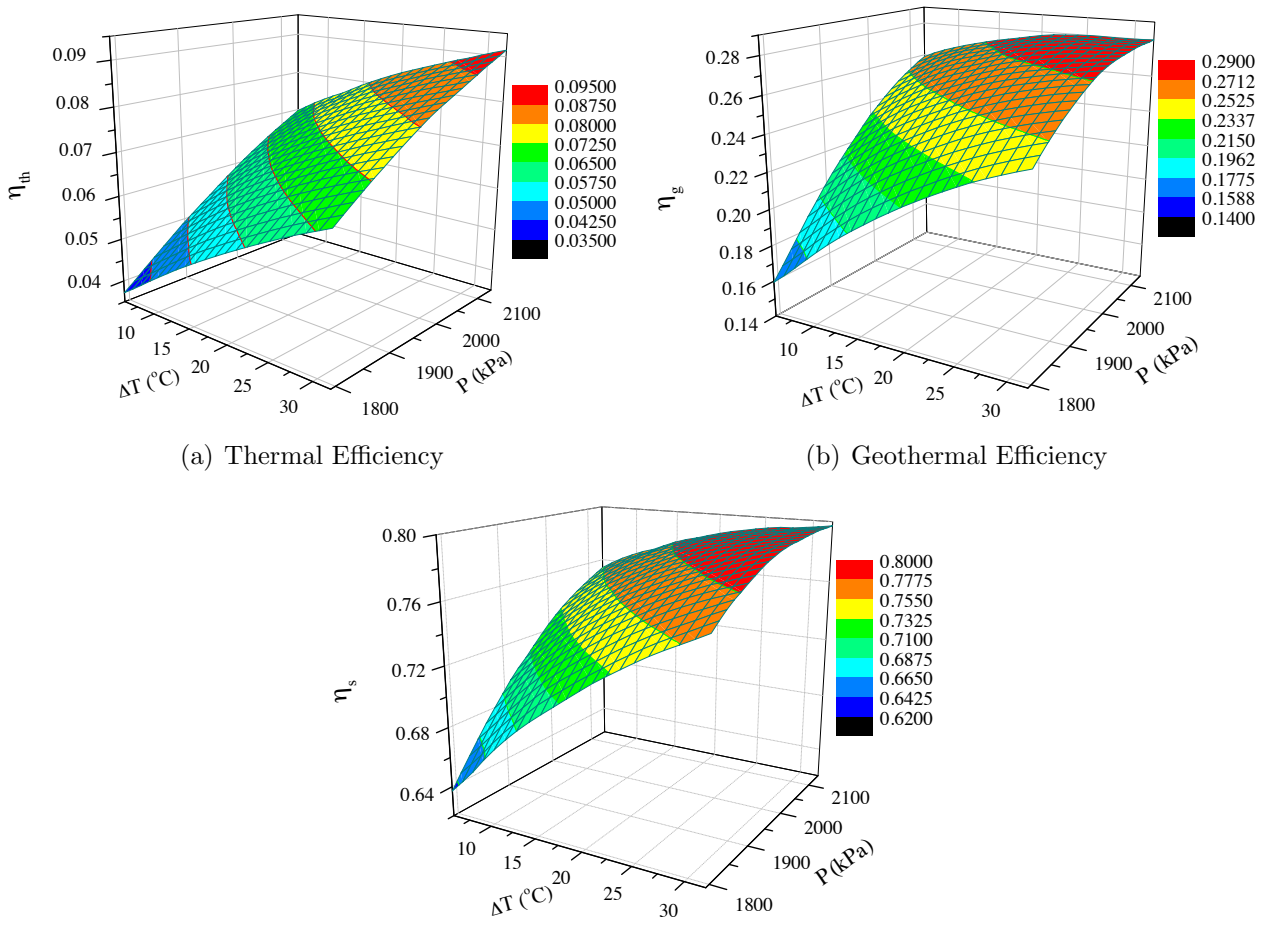

(a) Thermal Efficiency

(b) Geothermal Efficiency

(c) Isentropic Efficiency

Figure 13: The values of η_I, $\eta_{II,g}$, and η_s of turbine are shown as functions of the two independent variables for T_{amb}=26.7 ℃. The colored mesh represents magnitude of the efficiencies.

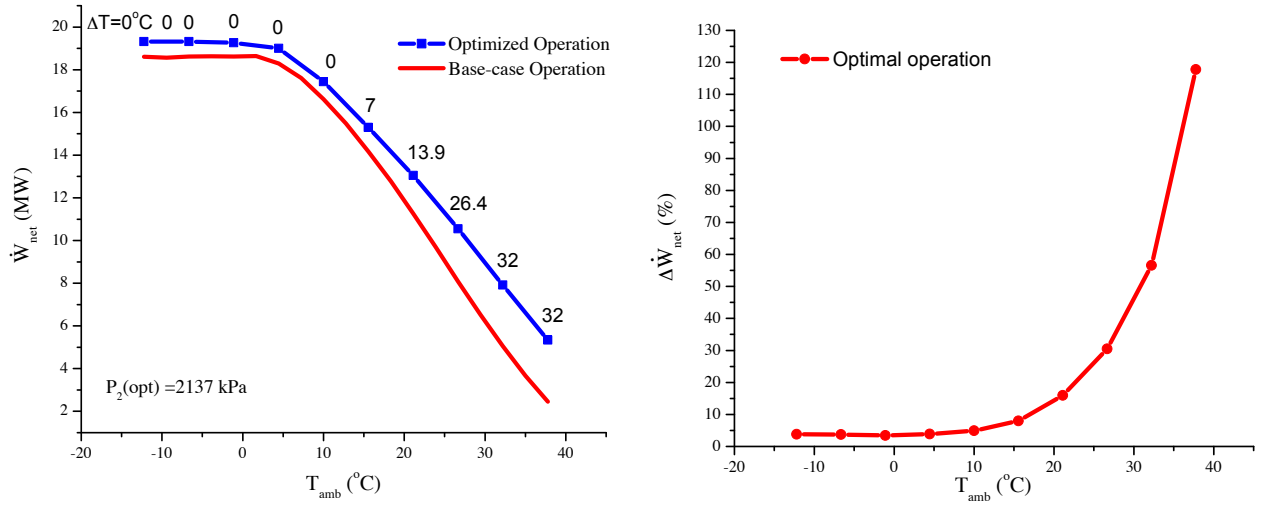

(a) (b)

Figure 14: (a) The optimum values of objective function are compared with the base-case operations as a function of T_{amb}. The value of P_2 for optimal operation is shown and the value of ΔT_{tu} is indicated for some optimum conditions. As mentioned above, the value of ΔT_{tu} for the base-case is 8 ℃. Note that at high T_{amb}, the value of ΔT_{tu} is limited by the inlet temperature of brine in the vaporizer. (b) The percentage increase in the net power output of the system compared to the base-case operation is shown. Note that at high T_{amb}, optimal operation of the system offers a significant increase in the net power output.

the inlet temperature of brine in the vaporizer. The percentage increase in the power output of the ORC is defined as

$$\Delta \dot{W}_{net} = \frac{\dot{W}_{net}^{Opt} - \dot{W}_{net}}{\dot{W}_{net}} \times 100$$

The values of $\Delta \dot{W}_{net}$ as a function of T_{amb} are shown in Fig. 14(b). Note that at high ambient temperatures, optimal operation offers up to 19% more $\dot{W}_{net}$ compared to the case of four fans in Fig. 9. In other words, a simple change in operation can give higher benefits, than adding cooling capacity, which involves substantial capital costs.

If one compares the η_s curves presented in Figs. 11 and 13, one finds that η_s is independent of ΔT_{tu} in Fig. 11 (low T_{amb}) and a monotonic increasing function of ΔT_{tu} in Fig. 13 (high T_{amb}). When η_s is constant, maximal power generation is achieved by keeping the inlet condition of turbine at the vapor saturation line as suggested by the previous studies [6, 18]. However, when η_s is not constant (affected by cooling capacity of ACC), the optimal operation of the system

Table 1: The properties of the streams at optimal operation for ΔT_{tu}=32 ℃ and P=2137 kPa at T_{amb}=26.7 ℃ are presented.

Stream	Fluid	T ℃	P kPa	$\dot{m}$ kg/s	V_{Frac}	h kJ/kg
IBL-1	Isobutane	39.5	532.6	1426	0	-2632
IBL-3	Isobutane	39.5	532.6	475	0	-2632
IBH-1	Isobutane	40.7	2137	475	0	-2628
IBH-4	Isobutane	40.7	2137	713	0	-2628
IBH-6	Isobutane	69.3	2126	713	0	-2553
IBH-8	Isobutane	69.3	2127	1426	0	-2553
IBH-9	Isobutane	102.0	2061	1426	0.084	-2437
IBH-10	Isobutane	132.2	1994	1426	1	-2164
IBL-6	Isobutane	93.5	541	713	1	-2213
IBL-8	Isobutane	56.2	540	713	1	-2288
IBL-10	Isobutane	40.4	537	713	0.68	-2418
IBL-11	Isobutane	40.3	535	713	0.31	-2534
Air1	Air	26.7	87.9	6478	1	1.7
Air2	Air	41.0	87.9	6478	1	16.0
Air3	Air	26.7	87.9	6512	1	1.7
Air4	Air	39.2	87.9	6512	1	14.3
Air5	Air	26.7	87.9	5566	1	1.7
Air6	Air	39.3	87.9	5566	1	14.3

is achieved when η_s is maximum. The table of streams for the optimal condition at T_{amb}=26.7 ℃ is presented in Table. 1.

To investigate the effect of optimal operation in the total power production of the plant, we obtained the ambient temperature and power production data for one year (Nov. 2010-Nov. 2011). The frequency distribution of ambient temperature for one year is shown in Fig. 15(a). For this time period, the power production in the base-case and optimal operations are compared and shown in Fig. 15(b). These results suggest that the total power production in this plant can be increased by 9% by optimal operation of the plant without any modification of the design. This is a significant improvement in the operation of the plant. Based on the electricity price data (Fixed price throughout the year) provided by ENEL, we found that the optimal operation can increase the revenue of the plant by 10.2%. Note that the majority of the increase is for hot ambient temperature, which are typically correlated with high value/price

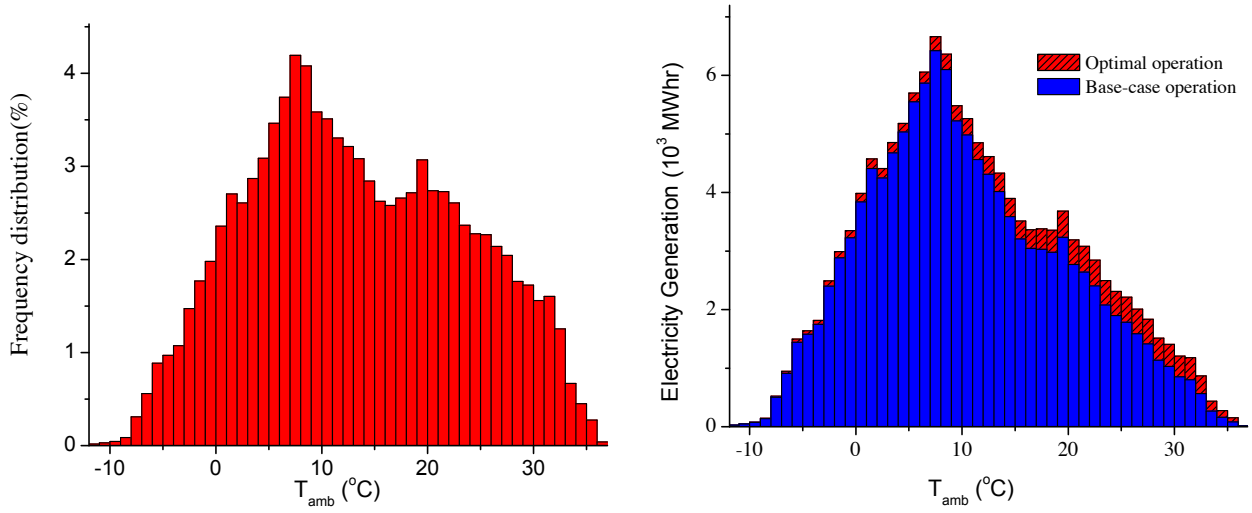

(a) (b)

Figure 15: (a) The frequency distribution of the ambient temperature for one year is shown. (b) The total power production in the base-case operation and the optimal operation are compared. The optimal operation offers 9% increase in the total power production.

of electricity, and thus the economic benefit is even higher.

As mentioned earlier, f_f can be considered as an optimization variable when $T_{amb} \leq 1.7$ ℃. For this range of ambient temperature, the ACC system does not limit the maximum of $\dot{W}_{net}$ of the ORC. Thus, the optimal operation is achieved when state 4 is at the saturation vapor line and the maximum feasible pressure. For $T_{amb} \leq 1.7$ ℃, by fixing state 4, the optimum value of $\dot{W}_{net}$ is found by considering f_f as the optimization variable. The results are presented in Fig. 16. As shown, at low ambient temperatures, the drive frequency of VFD fans should be adjusted to obtain the maximum of $\dot{W}_{net}$.

6. Optimization of the operation of the ORC: A fast shortcut method

In this section an alternative approach is presented to determine the optimal operation of the ORC at different ambient temperatures assuming constant pinches in the HXs. This approach is faster and easier to implement compared to the optimization in Aspen Plus. However, it does not provide a detailed analysis on the different components of the ORC nor it does account for

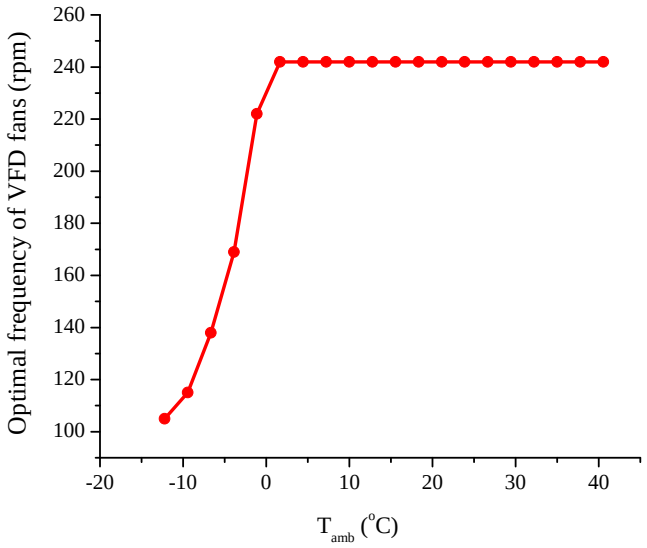

Figure 16: The optimal values of drive frequency of VFD fans are shown as a function of T_{amb}. when $T_{amb} \geq 1.7$ ℃, all the VFD fans should be kept at the maximum load. However, when $T_{amb} \leq 1.7$ ℃, the drive frequency of VFD fans should be adjusted to obtain the optimal values of outlet pressure of turbine and the maximum of $\dot{W}_{net}$.

all parasitic terms (Pressure drop).

This approach uses the pinch conditions at the vaporizer and the condensers. As an example, the pinch conditions at the vaporizer+preheater (Fig. 17(a)) and the constant frequency drive condenser (Fig. 17(b)) for the base-case operation (without optimization) of the studied ORC at T_{amb}= 26.7 ℃ are presented. Note that the pinches always occur at these points, saturated liquid point at the vaporizer+preheater and the outlet of the condenser.

The pinch condition at the vaporizer is used to determine the mass flow rate of WF ($\dot{m}^{WF}$) in the ORC and the pinch condition at the condenser is applied to determine the condensation pressure. For a given inlet pressure of WF (P_4), the energy balance between the pinch point and the outlet of the vaporizer gives

$$\dot{m}^{GB}(h_{in}^{GB}(T_{in}^{GB}, P_{in}^{GB}) - h_p^{GB}(T_p^{GB}, P_p^{GB})) = \dot{m}^{WF}(h_4(T_4, P_4) - h_p(P_4)) \tag{12}$$

where subscript p denotes the evaluated properties at the pinch point. For a given pinch of

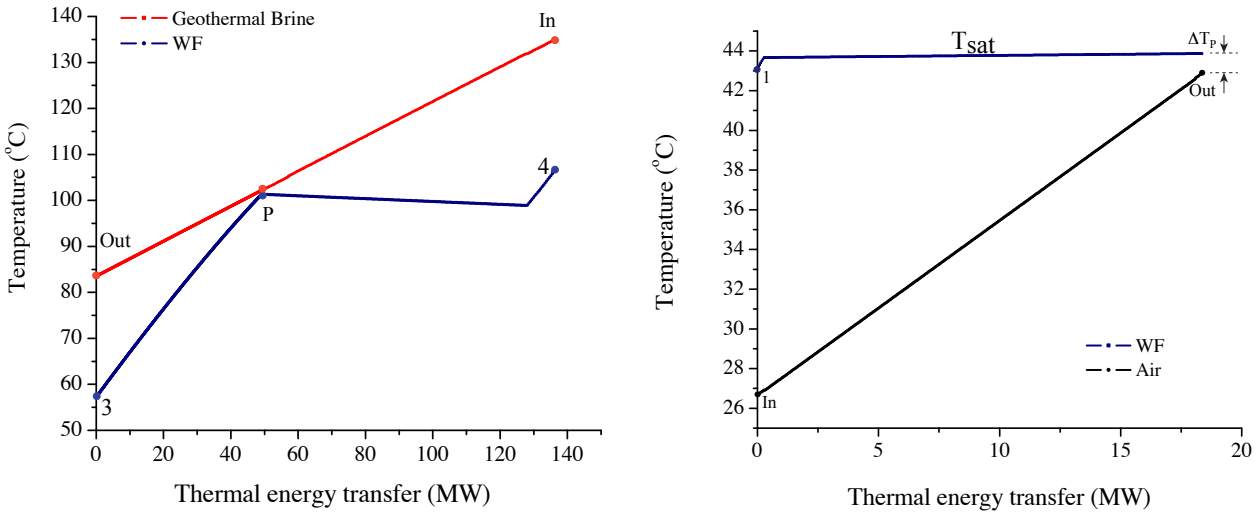

(a) Pinch at the vaporizer+preheater

(b) Pinch at the last condenser

Figure 17: The pinch conditions at the vaporizer and the condenser for the base-case operation of the ORC at T_{amb}=26.7 ℃ are shown. These conditions are used to determine the mass flow rate of WF ($\dot{m}^{WF}$) and condensation pressure (P_5) in the ORC. Note that due to the pressure drop in the condenser, the temperature line of the WF is not flat.

ΔT_p, one can write

$$T_p^{GB} = T_p^{WF} + \Delta T_p. \tag{13}$$

In addition, for a pinch point at the vaporizer, T_p^{WF} can be determined by the given value of P_4 and expressed as

$$T_p^{WF} = T^{sat}(P_4) \tag{14}$$

Since for a given geothermal energy source, the values of $\dot{m}^{GB}$, T_{in}^{GB} and P_{in}^{GB} are given, the left hand-side of the Eq.12 is known. Thus, for a given P_4, there are two unknowns in Eq. 12. For a turbine designed for a specific flow rate and enthalpy drop, there is a correlation between the independent variables at the inlet and the outlet of the turbine

$$g(\dot{m}^{WF}, T_4, P_4, T_5, P_5) = 0. \tag{15}$$

This equation along with Eq. 12 provide two equations with three unknowns, (T_4, P_5 and $\dot{m}^{WF}$). Another equation should be added to this system of equations to solve for the unknown variables and this is the functional dependence of outlet pressure of the turbine to the mass flow rate of WF.

Once a pinch condition occurs in the condenser, the outlet pressure of the turbine and consequently the condensation temperature is limited by the outlet temperature of cooling medium, Fig. 17b. Here, we consider an ACC for the analysis, but this approach can be applied to other condensers as well. For the pinch condition at the condenser, assuming constant properties of air, one can write

$$\dot{m}^{air} C_p^{air} (T^{sat} - \Delta T_p - T_{amb}) = \dot{m}^{WF} (\Delta x h_{fg} + \Delta h^L) \tag{16}$$

where Δx denotes the difference in quality of WF at the inlet and outlet of the condenser and Δh^L the enthalpy change of WF due to subcooling. For a single condenser, the value of Δx is 1 and for multiple condensers in series, $\Delta x \leq 1$. At a given T_{amb}, three assumptions are made to simplify Eq. 16,

$$\begin{aligned} \dot{m}^{air} C_p^{air} &= Const. \\ h_{fg} &= a P_5 + b \\ T^{sat}(P_5) &= T^{sat}(P_5^o) + \left(\frac{\mathrm{d}T^{sat}}{\mathrm{d}P_5}\right)_{P_5^0} (P_5 - P_5^o) \end{aligned} \tag{17}$$

where P_5^o denotes the outlet pressure of turbine at the base-case operation. Approximation of h_{fg} as a linear function of P_5 gives an error of ≈ 0.5 % for the range of P= 270-830 kPa. The values of a and b are dependent upon the WF properties; for the case herein (isobutane), they are given in Table 2. Applying these assumptions to Eq. 16, we obtain

$$\left(\frac{\dot{m}^{air} C_p^{air}}{a \Delta x}\right) \left(T^{sat}(P_5^o) + \left(\frac{\mathrm{d}T^{sat}}{\mathrm{d}P_5}\right)_{P_5^0} (P_5 - P_5^o) - \Delta T_p - T_{amb}\right) = \dot{m}^{WF} \left(P_5 + \frac{b}{a} + \frac{\Delta h^L}{a \Delta x}\right) \tag{18}$$

or equivalently

$$P_5 = \frac{C_1 - C_3 \dot{m}^{WF}}{\dot{m}^{WF} - C_2} \tag{19}$$

where

$$\begin{aligned} C_1 &= \left(\frac{\dot{m}^{air} C_p^{air}}{\Delta x a}\right) \times (T^{sat}(P_5^o) - \left(\frac{\mathrm{d}T^{sat}}{\mathrm{d}P_5}\right)_{P_5^o} P_5^o - \Delta T_p - T_{amb}) \\ C_2 &= \left(\frac{\dot{m}^{air} C_p^{air}}{\Delta x a}\right) \left(\frac{\mathrm{d}T^{sat}}{\mathrm{d}P_5}\right)_{P_5^o} \\ C_3 &= \frac{b}{a} + \frac{\Delta h^L}{\Delta x a} \end{aligned} \tag{20}$$

Eq. 19 suggests a simple correlation between the outlet pressure of turbine and the mass flow rate of WF. According to this equation, at a given T_{amb}, by having base-case operation data (by Aspen Plus simulator), one can determine the outlet pressure of the turbine based on the mass flow rate of WF in different operations. This equation should be validated before coupling with the equations derived above (Eqs. 12 and 15). In the geothermal system studied above, the last air-cooled condenser is chosen to examine Eq. 19. For three ambient temperatures, T_{amb}=10, 21.11 and 37.77 ℃, the value of C_1, C_2 and C_3 are determined from a simulation of base-case operation. These values are tabulated in Table. 2. We note that the value of C_1 is sensitive to the $T^{sat}(P_5^o)$ and ΔT_p. Thus, to keep high accuracy in the predictions, the value of C_1 is determined by the given values of P_5^o and $\dot{m}^{WF}$ at the base-case operation. The predicted outlet pressure of turbine as a function of mass flow rate by Eq. 19 and the simulated values by Aspen Plus are compared and shown in Fig. 18. There is a good agreement between the predicted outlet pressure of turbine with the simulated values, Fig. 18.

Equation 19 is considered with Eqs. 12 and 15 to form a system of equations for a given T_4 and P_4 (or ΔT_{tu} and P_4). This system of equations can be solved numerically. Here, we have used EES software for this calculation, since libraries of thermodynamic properties for different

Table 2: The constants of Eq. 19 are determined at three ambient temperatures (T_{amb}=10, 21.11 and 37.77 ℃). The values of a and b for Isobutane are -0.0844 and 357.3, respectively. The value of ΔT_P is 1 ℃.

T_{amb} ℃	P_5^o kPa	$\dot{m}^{WF-o}$ kg/s	$\dot{m}^{air}$ kg/s	C_p^{air} kJ/(kgK)	$\left(\frac{\mathrm{d}T^{sat}}{\mathrm{d}P}\right)_{P_5^o}$ K/(kPa)	Δx	Δh^L kJ/kg	C_1 $\times 10^{-5}$	C_2	C_3
10	384	190.8	1201	1.006	0.0916	0.31	2.3	8.72734	-4229.92	-4321.32
21.11	518	190.51	1154	1.007	0.0731	0.31	2.3	9.53116	-3238.77	-4321.32
37.77	777	191.39	1095	1.007	0.0544	0.31	2.3	11.00868	-2289.85	-4321.32

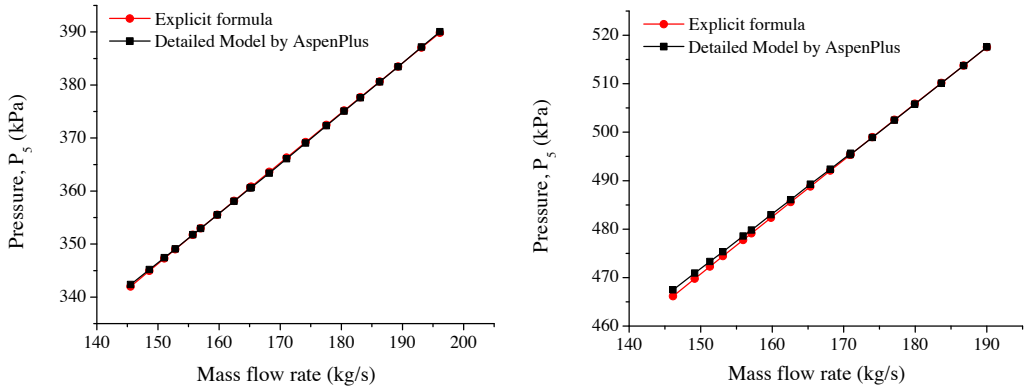

(a) T_{amb}=10 ℃ (b) T_{amb}=21.11 ℃

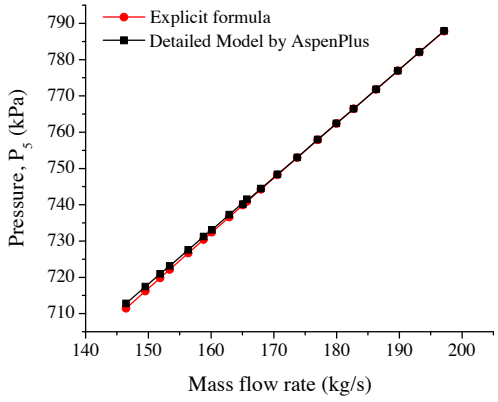

(c) T_{amb}=37.77 ℃

Figure 18: The predicted outlet pressures of the turbine as a function of the mass flow rate from Eq. 19 is compared with the simulated values by Aspen Plus at three ambient temperatures. Note that the values of mass flow rate can be converted as the values of ΔT_{tu} through Eq. 12.

Table 3: The volumetric flow rate through the pumps for the optimum operating condition at T_{amb}=32.2 ℃ is presented.

ΔT_{tu} (℃)	P (kPa)	$\dot{V}_{WF}$ (m^3/hr)	$\dot{V}_A$ (m^3/hr)	fr(A) (rpm)	$\dot{V}_B$ (m^3/hr)	$\dot{V}_C$ (m^3/hr)
32	2137	1838	472	1700	682	682

fluids are built in. The value of $\dot{W}_{net}$ of the ORC is expressed as

$$\dot{W}_{net} = 2 \times \dot{m}^{WF}(h_4 - h_5) - \dot{W}_{pa} \tag{21}$$

For $T_{amb} \geq 1.7$ ℃, parasitic power of the fans is approximately constant and the dependence of parasitic power of the pumps on the mass flow rate of WF is included in Eq. 21. Thus, by solving the system of equations discussed above, one can determine the value of $\dot{W}_{net}$. An iterative approach is adopted to determine the optimal value of ΔT_{tu} at a given P_4 maximizing $\dot{W}_{net}$ of the ORC. At the maximum value of P_4, for each value of ΔT_{tu}, the system of equations are solved and the value of $\dot{W}_{net}$ is compared with the previous values to determine the maximum point. Note that the developed approach solves Eq. 10 for a given value of P_2 at the maximum value of f_f. For $T_{amb} \geq 1.7$ ℃, as discussed above, the value of $\dot{W}_{net}$ remains constant. The results of this approach are compared with the optimization results from Aspen Plus in Figs. 19 and 20. There is a good agreement between the results obtained by these two independent approaches. The difference is related to the pressure drop effect considered in Aspen Plus model. The advantage of the new approach implemented in EES is a much shorter convergence time. However, the new approach is not as detailed as optimization in Aspen Plus and cannot provide values of thermodynamic properties in the intermediate states.

Once the optimum operation rules are found, one can use Fig. 4 to find the flow rate through each pump. For the case of T_{amb}=32.2 ℃, the flow rates through each pump is tabulated in Table. 3.

Since geothermal sources are depleting over time, one could take the depletion rate of the geothermal source ($\dot{m}_{GB}$ and T_{GB}) into account. The optimal operation depends on the T_{GB}.

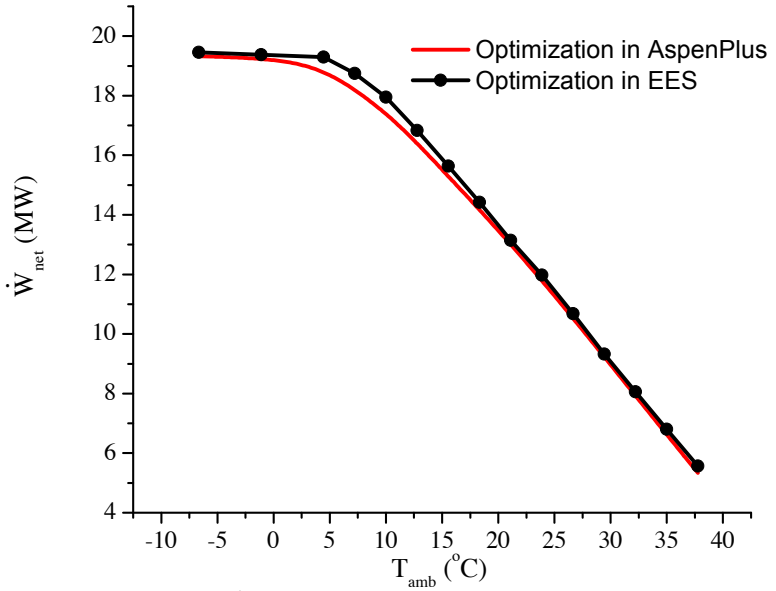

Figure 19: The maximum value of $\dot{W}_{net}$ at P_4=2137 kPa is determined by two approaches; detailed model in Aspen Plus and shortcut approach implemented in EES. The difference is related to the pressure drop effect considered in Aspen Plus model. Note that method 2 has much shorter convergence time.

The model implemented in EES is used to determine the new optimal operation. When the brine temperature drops by 5 ℃, the maximum drop in $\dot{W}_{net}$ of the system occurs at high ambient temperatures (up to 15%).

7. Conclusions

For an existing ORC equipped with an ACC system and utilizing a low temperature geothermal source, a simulator has been developed in Aspen Plus. This simulator includes the actual characteristics of all the components of an existing cycle. The simulator is validated with a set of approximately 5000 measured data. The simulator suggests that at high ambient temperatures, the net power output of the ORC is limited by the capacity of ACC system. This limitation could be mitigated by incorporation of more fans in the ACC system or by better operation strategy. We found that optimal operation strategies provide the same scale increase in net power (up to 117 %) as incorporation of more fans in the ACC system. The former

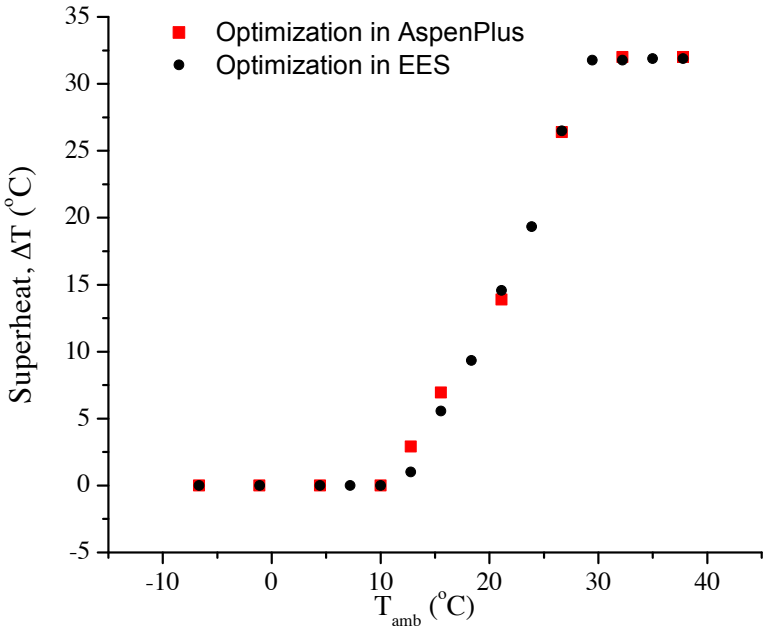

Figure 20: The optimal values of ΔT_{tu} determined by two independent approaches are compared at different T_{amb}. The agreement between the results suggest that the second approach which is faster can be used instead of optimization by Aspen Plus to determine the optimal operation. However, the second approach is not as detailed as the first approach.

is clearly favorable since it does not require additional capital cost expenditure. The overall increase in electricity generation (MWhr) over the course of a year is ≈ 9 %, with most of the increase for high ambient temperature, i.e., at times where electricity is more valuable.

The operation of this ORC is optimized maximizing the net power output of the ORC. The optimal operation suggests that at low ambient temperatures, the inlet of turbine should be in a saturated vapor state and the maximum feasible pressure as suggested by previous studies [6, 18]. However, interestingly, as the ambient temperature increases, this conclusion does not hold anymore and a significant superheat is required to obtain the maximum in net power output of the ORC. This is consequence of the off-maximum operation of the turbines and consequently variable isentropic efficiency. As expected, at high ambient temperatures, the ACC system should be at full capacity for the optimal operation, but at low ambient temperatures, the cooling capacity of the ACC system should be adjusted to obtain the optimal operation.

A shortcut approach is developed to determine the optimal operation of an ORC and implemented in EES. This approach is based on the pinch conditions at the vaporizer and the condenser and isentropic equation of the turbine; it has much shorter convergence time compared to the Aspen Plus simulator, but requires some of the base-case operation data simulated in Aspen Plus. The results of this approach are in a good agreement with the ones obtained by Aspen Plus simulator. From the pinch condition at the condenser, for a given condensation system, a simple explicit formula is derived that correlates the outlet pressure of the turbine to the mass flow rate of WF in an ORC. This formula is validated by the results from the simulations. This formula can be applied to other condensation systems once the characteristics of the condenser are known.

Acknowledgment: This work is conducted with the financial support from ENEL. Hadi Ghasemi gratefully acknowledges his Postdoctoral Fellowship through the Natural Sciences and Engineering Research Council of Canada (NSERC). Aspen Plus was generously provided by Aspen Technology. The authors would like to thank Randall Field and Nicola Rossi and his

team at ENEL for their useful inputs.

References

[1] Lund H. Renewable energy strategies for sustainable development. Energy 2007;32:912–9.

[2] Delgado-Torres AM, García-Rodríguez L. Analysis and optimization of the low-temperature solar organic Rankine cycle (ORC). Energy Conversion and Management 2010;51:2846–56.

[3] Taljan G, Verbič G, Pantoš M, Sakulin M, Fickert L. Optimal sizing of biomass-fired organic Rankine cycle CHP system with heat storage. Renewable Energy 2012;41:29–38.

[4] Yamamoto T, Furuhata T, Arai N, Mori K. Design and testing of the organic Rankine cycle. Energy 2001;26:239–51.

[5] Yari M. Exergetic analysis of various types of geothermal power plants. Renewable Energy 2010;35:112–21.

[6] Saleh B, Koglbauer G, Wendland M, Fischer J. Working fluids for low-temperature organic Rankine cycles. Energy 2007;32:1210–21.

[7] Li J, Pei G, Li Y, Wang D, Ji J. Energetic and exergetic investigation of an organic Rankine cycle at different heat source temperatures. Energy 2012;38:85–95.

[8] Roya J, Mishra M, Misra A. Parametric optimization and performance analysis of a waste heat recovery system using organic rankine cycle. Energy 2010;35:5049–62.

[9] Sun J, Li W. Operation optimization of an organic Rankine cycle (ORC) heat recovery power plant. Applied Thermal Engineering 2011;31:2032–41.

[10] Hettiarachchia HM, Golubovica M, Woreka WM, Ikegamib Y. Optimum design criteria for an organic Rankine cycle using low-temperature geothermal heat sources. Energy 2007;32:1698–706.

[11] Angelino G, Paliano PCD. Multicomponent working fluids for organic Rankine cycles (ORCs). Energy 1998;23(6):449–63.

[12] Dai Y, Wang J, Gao L. Parametric optimization and comparative study of organic Rankine cycle (ORC) for low grade waste heat recovery. Energy Conversion and Management 2009;50:576–82.

[13] Heberle F, Brüggemann D. Exergy based fluid selection for a geothermal organic Rankine cycle for combined heat and power generation. Applied Thermal Engineering 2010;30:1326–32.

[14] He C, Liu C, Gao H, Xie H, Li Y, Wu S, et al. The optimal evaporation temperature and working fluids for subcritical organic Rankine cycle. Energy 2012;38:136–43.

[15] Hung TC, Shai TY, Wang SK. A review of organic Rankine cycles for the recovery of low-grade waste heat. Energy 1997;22:661–7.

[16] Lai NA, Wendland M, Fischer J. Working fluids for high-temperature organic Rankine cycles. Energy 2011;36(199-211).

[17] Liu BT, Chien KH, Wang CC. Effect of working fluids on organic Rankine cycle for waste heat recovery. Energy 2004;29:1207–17.

[18] Mago PJ, Chamra LM, Srinivasan K, Somayaji C. An examination of regenerative organic Rankine cycles using dry fluids. Applied Thermal Engineering 2008;28:998–1007.

[19] Schuster A, Karellas S, Aumann R. Efficiency optimization potential in supercritical organic Rankine cycles. Energy 2010;35:1033–9.

[20] Wang E, Zhang H, Fan B, Ouyang M, Zhao Y, Mu Q. Study of working fluid selection of organic Rankine cycle (ORC) for engine waste heat recovery. Energy 2011;36:3406–18.

[21] Pan L, Wang H, Shi W. Performance analysis in near-critical conditions of organic Rankine cycle. Energy 2012;37:281–6.

[22] Papadopoulos AI, Stijepovic M, Linke P. On the systematic design and selection of optimal working fluids for organic Rankine cycles. Applied Thermal Engineering 2010;30:760–9.

[23] Schuster A, Karellas S, Kakaras E, Spliethoff H. Energetic and economic investigation of organic Rankine cycle applications. Applied Thermal Engineering 2009;29:1809–17.

[24] Milora SL, Tester JW. Geothermal energy as a source of electric power. The MIT Press, Cambridge, Massachusetts; 1976.

[25] Zebian H, Gazzino M, Mitsos A. Multi-variable optimization of pressurized oxy-coal combustion. Energy 2012;38:37–57.

[26] Serth RW. Process heat transfer: Principles and applications. Academic Press: New York; 2007.

[27] Kern DQ. Process heat transfer. McGraw-Hill; 1950.

[28] Kern DQ, Kraus AD. Extended surface heat transfer. McGraw-Hill; 1972.

[29] Palen JW. Shell and tube reboilers, in heat exchanger design hanbook; vol. 3. Hemisphere Publishing Corp.; 1988.

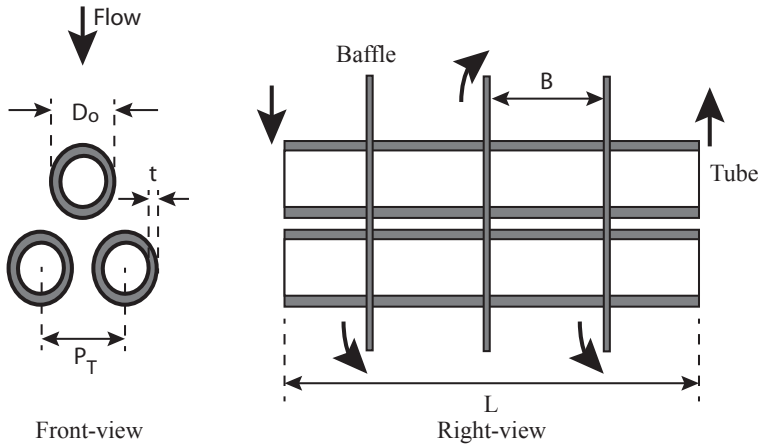

Figure 21: A layout of tubes in a Shell and tube heat exchanger is shown. The geometrical dimensions of the heat exchangers in the studied system are listed in Table 4.

Table 4: The dimensions of the heat exchangers

Component	Type	Material	L mm	D_s mm	D_o mm	t mm	N_T	P_T mm	B mm
Recuperator	Shell and tube	C-Steel	5486.4	1981.2	31.75	2.11	2060	39.69	600.08
Preheater	Shell and tube	C-Steel	17678.4	1990.7	15.88	1.65	6137	20.64	1574.8
Vaporizer	Shell and tube	C-Steel	15849.6	1930.4	15.88	1.65	5180	20.64	1936.75
ACC	Tube	C-Steel	18288	–	31.75	2.11	6930	69.85	–
	Fin	Al	63.5	1.90	0.41	31.75			

8. Appendix

For the tube side of the heat exchangers including recuperators, preheaters, and vaporizers, the flow is a single phase. Thus, the heat transfer coefficient may be determined using Sieder-Tate and Hausen equations:[26]

For $Re > 10^4$

$$Nu = 0.023 \times Re^{0.8} \times Pr^{0.33} \times \left(\frac{\mu}{\mu_w}\right)^{0.14}. \tag{22}$$

The pressure drop in the tubes is expressed as the summation of major and minor losses [26–28]

$$\Delta P = \frac{f n_p L G^2}{2\rho D} + \frac{\alpha_r G^2}{2\rho}, \tag{23}$$

where the friction coefficient for the turbulent flow in the tubes may be written as

$$f = (0.790 \times \ln Re_{D_h} - 1.64)^{-2}, \tag{24}$$

and for turbulent flow and U-tubes [27]

$$\alpha_r = 1.6 n_p - 1.5.$$

For the shell side of heat exchangers, the heat transfer coefficient may be expressed as [26]

$$j_H = 0.5 \left(1 + \frac{L_B}{D_s}\right) (0.08 \times Re^{0.6821} + 0.7 \times Re^{0.1772})$$
$$Nu = j_H Pr^{1/3} \left(\frac{\mu}{\mu_w}\right)^{0.14}, \tag{25}$$

and the pressure drop on shell side of heat exchangers can be expressed as [26, 27]

$$\Delta P = \frac{f G_s^2 D_s (N_B + 1)}{\rho D_e \left(\frac{\mu}{\mu_w}\right)^{0.14}} + \frac{0.75 N_s G_n^2}{\rho}, \tag{26}$$

where

$$D_e = \frac{4(\beta P_T^2 - \pi D_0^2/4)}{\pi D_0}. \tag{27}$$

The value of β for square and triangular pitches are 1 and 0.86, respectively. The above correlations are for a single-phase flow. Once a phase change occurs in the heat exchangers, the transport of thermal energy depends on the thermodynamic states of all the present phases. For the boiling on the horizontal tubes, one may use Mostinski equation [29]

$$h_{c,nb} = 1.167 \times 10^{-8} P_c^{2.3} \Delta T_w^{2.333} F_p^{3.333}, \tag{28}$$

where

$$\Delta T_w = T_w - T^{sat}$$
$$F_p = 1.8P_r^{0.17} + 4 \times P_r^{1.2} + 10 \times P_r^{10}$$

For this case, some other empirical correlations exist [26]. Once there is a tube bundles in a heat exchanger, the heat transfer rate will be increased. This enhancement is caused by the convective circulation within and around the tube bundles. The recirculation is of buoyancy driven convection type and is driven by the density difference between the liquid surrounding the bundle and the two-phase mixture within the bundle. The increase in heat transfer rate can be determined by correlation suggested by Palen [29] and may be written as

$$h_{c,b} = h_{c,nb} \times F_b + h_{c,f} \tag{29}$$
$$h_{c,f} = 250,$$

where

$$F_b = 1 + 0.1\left(\frac{0.785 D_b}{C(P_T/D_o)^2 D_o} - 1\right)^{0.75},$$

where C is 0.866 and 1 for triangular and square layouts, respectively. For the condensation in horizontal tubes, one may use the Shah correlation [26] that can be written

$$h_c = 0.023 \times C \times Re_L^{0.8} \times Pr_L^{0.4} \frac{\kappa_L}{D_i}$$
$$C = (1-x)^{0.8} + 3.8x^{0.76}(1-x)^{0.04} \times (P/P_c)^{-0.38}. \tag{30}$$

For the air-side of ACC, heat transfer coefficient in the case of tube banks with three or more rows of tubes on triangular pitch and $\frac{A_{Tot}}{A_o} \leq 50$ can be written as [26]

$$Nu = 0.38 \times Re^{0.6} Pr^{1/3} \left(\frac{A_{tot}}{A_o}\right)^{-0.15}. \tag{31}$$

Once the heat transfer coefficients, for both sides of tubes are determined, the overall heat transfer coefficient for the heat exchangers may be written as

$$U_D = \left(\left[\frac{D_o}{h_{c,i} D_i} + \frac{D_o ln(D_o/D_i)}{2 \times \kappa} + \frac{1}{h_{c,o}} \right]^{-1} + R_D \right)^{-1} \tag{32}$$

For ACCs, the overall heat transfer coefficient may be written as [26]

$$U_D = \left[\left(\frac{1}{h_{c,i}} + R_{Di} \right) \frac{A_{tot}}{A_o} + \frac{A_{tot} \ln(D_o/D_i)}{2\pi\kappa_{tub} L} + \frac{A_{tot} ln(D_{o,sl}/D_{i,sl})}{2\pi\kappa_{sl} L} \right] + \left[\frac{R_{con} A_{tot}}{\pi D_o L} + \frac{1}{\eta_w h_{c,o}} + \frac{R_{Do}}{\eta_w} \right] \tag{33}$$

This correlation is introduced for bimetallic tubes. If the tube and fin are made of a same material, the term pertinent to sleeve should be ignored. For the sake of convenience, in this study, the contact resistance is ignored.